PLOS CLIMATE

RESEARCH ARTICLE

Tolerance of coralline algae to ocean warming and marine heatwaves

Erik C. Krieger[1]*, Aleluia Taise[1], Wendy A. Nelson[2,3], Johan Grand[4,5], Eric Le Ru[4], Simon K. Davy[1], Christopher E. Cornwall[1]

1 School of Biological Sciences, Victoria University of Wellington, Wellington, New Zealand, **2** School of Biological Sciences, University of Auckland, Auckland, New Zealand, **3** National Institute of Water and Atmospheric Research, Wellington, New Zealand, **4** School of Chemical and Physical Sciences, Victoria University of Wellington, Wellington, New Zealand, **5** Université de Paris, ITODYS, CNRS UMR 7086, Paris, France

* erik.krieger@vuw.ac.nz

Citation: Krieger EC, Taise A, Nelson WA, Grand J, Le Ru E, Davy SK, et al. (2023) Tolerance of coralline algae to ocean warming and marine heatwaves. PLOS Clim 2(1): e0000092. https://doi.org/10.1371/journal.pclm.0000092

Editor: Ming Li, University of Maryland Center for Environmental Science, UNITED STATES

Received: March 19, 2022

Accepted: November 4, 2022

Published: January 4, 2023

Data Availability Statement: All relevant data can be accessed here: https://doi.org/10.5061/dryad.jwstqjqdh.

Funding: ECK and CEC were supported by a Rutherford Discovery Fellowship from The Royal Society of New Zealand Te Apārangi (no. RDF-VUW1701) awarded to CEC. Part of the research was paid for by a grant awarded to CEC and WAN by the Victoria University of Wellington University Research Fund. The funders had no role in study design, data collection and analysis, decision to publish, or preparation of the manuscript.

Abstract

Ocean warming (OW) and marine heatwaves (MHWs) rapidly transform marine ecosystems, especially when they impact keystone or foundation species. Foundation species such as kelps, fucoids and corals are highly sensitive to heat stress, which threatens the future of temperate seaweed forests and tropical reefs. However, functioning and resilience of these systems also relies on the less conspicuous coralline algae, whose thermal tolerances have gone largely untested. Here, we examined the sensitivity of four temperate coralline algal morphotypes from three different species to four realistic present day and future OW and MHW scenarios (ambient [16˚C constant]; ambient+MHW [16˚C baseline + a symmetric two-week heatwave with a peak intensity of 18.7˚C]; future [18.7˚C constant]; future +MHW [18.7˚C baseline + a symmetric two-week heatwave with a peak intensity of 21.4˚C]). Photo-physiology (e.g., Fv/Fm) and calcification physiology (e.g., proxies for calcifying fluid saturation state Ω_{CF}) were generally unaffected by the treatments, implying a high thermo-tolerance of our study species compared to other important marine foundation species. We ascribe this mainly to their photosynthetic apparatus that, unlike in other photoautotrophs, continued to function under heat stress. Experimental evidence presented here and elsewhere implies that coralline algae are likely to continue to play their crucial ecological roles in a warming ocean. Yet, such predictions are fraught with uncertainty due to the substantial gaps in our knowledge. We attempt to highlight some of these gaps and aim to present potential physiological underpinnings of their thermo-tolerance.

1 Introduction

Coralline algae are important engineers of biogenic reefs and other benthic ecosystems across all latitudes and throughout the photic zone [1, 2]. In temperate and subpolar regions, coralline algae monopolise the understory below the canopy formed by larger brown algae [3–5]. The positive interactions between the two functional guilds promote their coexistence and are key for the functioning of these seaweed forests [5, 6]. In the tropics, coralline algae are crucial for

Competing interests: The authors have declared that no competing interests exist.

the construction of coral reefs, acting as consolidators and binders of the reef framework [7–11]. However, coralline algae not only support coral reefs but also construct extensive reef systems of their own [12–15]. In addition to being important foundation taxa, coralline algae act as settlement substrate for many invertebrates, including corals, abalone and sea urchins [16–19]. The ability of coralline algae to play these important ecological roles is threatened by global change, especially ocean acidification [20]. Yet, how coralline algae will respond to ocean warming is relatively uncertain given the comparably low number of studies and the contrasting results. For example, reported impacts of ocean warming on coralline algal photosynthesis and calcification range from negative [21, 22] over neutral [23, 24] to positive [25, 26]. In addition, responses of coralline algae to marine heatwaves are virtually unknown [27]. Given their high ecological importance, it is crucial that we gain a better understanding regarding the effects of ocean warming, marine heatwaves, and their interactive effects on coralline algae. Increasing this understanding is the aim of this study.

Rising anthropogenic greenhouse gas forcing is progressively heating the world's oceans [28–30]. Over the last 170 years, the average temperatures of the surface ocean (SST) have increased by 0.88˚C and will continue to rise over the 21st Century [31]. It is projected that by 2100, mean SST will have increased further by at least 0.86˚C (SSP1-2.6) and up to 2.89˚C (SSP5-8.5) [31]. Concurrent with ocean warming (OW), local extreme temperature events (marine heatwave, MHWs) have also increased in duration, frequency, and intensity [32]. This is a trend that will accelerate with further ocean warming [33, 34].

Ocean warming and marine heatwaves negatively impact many marine biota, including sensitive foundation species such as coral and kelp [35, 36] but whether coralline algae are equally susceptible is unclear. Many habitat-forming kelps and fucoids exposed to acute or chronic thermal stress exhibit heat-related decreases in chlorophyll content, and photosynthetic efficiency and output, indicating thermally-induced damage of the photosynthetic apparatus [37–40]. As a result, growth often declines and mortality tends to increase [37, 41]. For coralline algae, such observations are, in comparison, sparse. However, there have been reports of reduced calcification and increased mortality in coralline algae due to heat-induced bleaching [21, 42]. Yet, the occurrence of thermally-induced bleaching is inconsistent and in some cases elevated temperatures have had either no or positive impacts on coralline algal physiology [24–26]. Additionally, the link between temperature dependent bleaching and reduced calcification can be weak [22, 42, 43]. Further, many other causes such as light and handling stress have been linked with bleaching in coralline algae (e.g., [44]) which could have influenced earlier observations of bleaching in laboratory settings. Coralline algal bleaching is different to coral bleaching as it refers to the degradation of photosynthetic pigments [45], commonly followed by necrosis and death, and not the expulsion of endosymbionts that occurs in corals. Also, limited data suggests that coralline algal communities in the field do not seem to respond, like coral, with mass bleaching in response to MHWs [15, 27, 46]. For example, during the 2016 mass coral bleaching event in Western Australia, coral communities underwent between 29 and 80.6% mortality, whereas coralline algae in the same regions were seemingly unaffected [15]. Thus, there is the potential that coralline algae could buffer [8, 9, 18] some of the ecological impacts associated with the global decline in live coral cover [47–49] caused by more frequent and intense mass coral bleaching and mortality events [50, 51].

Tropical coral reefs and temperate kelp forests are extremely diverse and productive ecosystems that are threatened by OW and MHWs due to sensitivity of the dominant foundation species (coral and kelps/fucoids) to thermal stress. However, resilience and future functioning of these systems also depends on the much less conspicuous coralline algae. Yet, information regarding their thermal sensitivity is severely lacking. Thus, we investigated the impact of ocean warming and marine heatwaves and their interaction on photo-physiology and

calcification of four temperate coralline algal morpho-types. We hypothesised that: (1) the chronic thermal stress associated with ocean warming will cause decreases in photosynthetic efficiency (Fv/Fm), pigment content (i.e., bleaching) and photosynthetic rates (approximated using electron transport rates), as well as decreased calcification rates and altered calcification physiology (mineralogy and crystal formation); (2) the expected negative impacts will be more pronounced under the acute heat stress of a marine heatwave; and (3) the interaction between acute and chronic heat stress will have the greatest negative impact on coralline algal calcification and photo-physiology.

2 Material and methods

2.1 Sample collection and field sites

Coralline algae were collected (Special Permit 711 issued to Victoria University of Wellington by the New Zealand Ministry of Primary Industries) by snorkellers around two months prior (4th March 2020) to the experiment from one field site located in Te Moana-o-Raukawa Cook Strait, Te Whanganui a Tara Wellington, Aotearoa New Zealand (41˚ 20' 55.7"S, 174˚ 47' 25.8"E; also see Site A/Sharks Tooth in Fig 1 in [52]). Since morphological identification of coralline algae is notoriously difficult, snorkellers were instructed to collect four morphologically distinct groups that *a priori* we considered most likely to be species or species complexes (for details regarding taxonomy see Section 2.2). These included one species of non-geniculate (*Phymatolithopsis* complex, N = 63), as well as three groups of geniculate coralline algae including two *Corallina* morpho-types from different depths (*Corallina* complex 1 sampled in the subtidal between 1–2 m deep, N = 70; *Corallina/Arthrocardia* "robust", N = 70; *Corallina* complex 2 sampled in the subtidal <1 m deep, N = 48). Mean dry weight of geniculate samples ranged between 0.36 and 0.46 g while crust covered rocks/cobbles were around 6 x 6 cm big with a mean dry weight of 38 g. For collection, geniculate coralline algae were chiselled from the rock with the attaching crust to avoid damaging them. Cobbles or rocks covered with crusts were collected directly from the seafloor. All samples were placed in separate resealable plastic bags filled with seawater while underwater, that were then placed in black plastic bags to reduce light stress and prevent physical damage before bringing them to the surface. After collection, organisms were transported to the laboratory facilities within 20 min in cooler bins filled with ice and cool packs, to further minimise thermal and light stress. At the laboratory, organisms were kept under low light (~8 μmol photons m^{-2} s^{-1} photosynthetically active radiation [PAR]) for two days to allow for slow acclimation to laboratory conditions. Light was then gradually increased to 80 μmol photons m^{-2} s^{-1} PAR over the course of fourteen days, during which organisms were also carefully cleaned of epibionts and labelled according to the morpho-anatomic classification. Epoxy (Z-Spar A-788 Splash Zone) was used to form a base for geniculate coralline algae. Specimens were then distributed into the experimental tanks. Each tank contained one or two specimens of at least three, but up to four, different species (for more details see S1 Table). After this initial sixteen-day period, organisms were kept for six weeks at around 16˚C which reflects the average temperatures in the field around the time of collection in late summer/early autumn temperatures. For most of this time, access to the laboratory facilities was not permitted due to COVID restrictions, with limited access only possible after week five. After this period, we started the experiment by beginning to increase the temperatures in the 'future' treatments over the course of one month (~0.1˚C d^{-1}). The experiment ran from the 11/05/2020 to the 28/07/2020 (79 days).

2.2 Species identification

To verify the taxonomic consistency of the species groups recognised using morph-anatomical characters (S1 Fig), five to seven specimens of each species (~10% of total samples) were

randomly selected for DNA-based identification (for further details regarding DNA extraction and sequencing please see [52]). The sequences obtained were compared to the findings of Twist et al. [53] and showed that none of the four groups was consistently identified to the species level using morpho-anatomic characteristics, reflecting the well-known difficulties of this approach [53, 54]. (Species codes below follow Twist et al. [53] and are based on sequence data and herbarium voucher material. Representative material has been deposited in the herbarium of the Museum of New Zealand Te Papa Tongarewa, Wellington, New Zealand [WELT].) The crustose samples grouped under *Phymatolithopsis* complex contained two species of Hapalidiales (*Phymatolithopsis repanda* (= *Hapalidiales* ZT ~85% and *Hapalidiales* sp. D ~15%). The geniculate group *Corallina/Arthrocardia* "robust" was revealed to consist of *Corallina* spp. (~60%) and *Arthrocardia* sp. C (~40%). The samples grouped as *Corallina* complex 1 included at least three closely related *Corallina* species (~20% *C. berteroi*, ~20% *C. chamberlainiae* and ~60% *C.* sp.) while the samples grouped as *Corallina* complex 2 also consisted solely of species from the genus *Corallina* (~20% *C. chamberlainiae* and ~80% *C.* sp.).

2.3 Experimental treatments and design

The study was conducted at the Wellington University Coastal Ecology Laboratory located on Wellington's Cook Strait coastline. The experiment consisted of four treatments each representing a different temperature regime (ambient; amb.+MHW; future; and fut.+MHW; see Fig 1). Ambient temperature was set to a constant 16˚C to reflect average temperatures encountered by the organisms at the time of collection in late summer/early autumn (S2 and S3 Figs). Future temperatures were set to a constant 18.7˚C to account for the projected increase of 2.73˚C in the global mean SST at the end of this century under the relative concentration pathway 8.5 [55]. The baseline temperatures in the two marine heatwave treatments were set to 16˚C and 18.7˚C respectively, but on top of this a symmetric two-week-long MHW was simulated after an exposure period of three weeks (t2–t4). The peak temperature (t5) of the MHW was set to 18.7˚C (amb.+MHW) and 21.4˚C (fut.+MHW), which reflects the strength of past

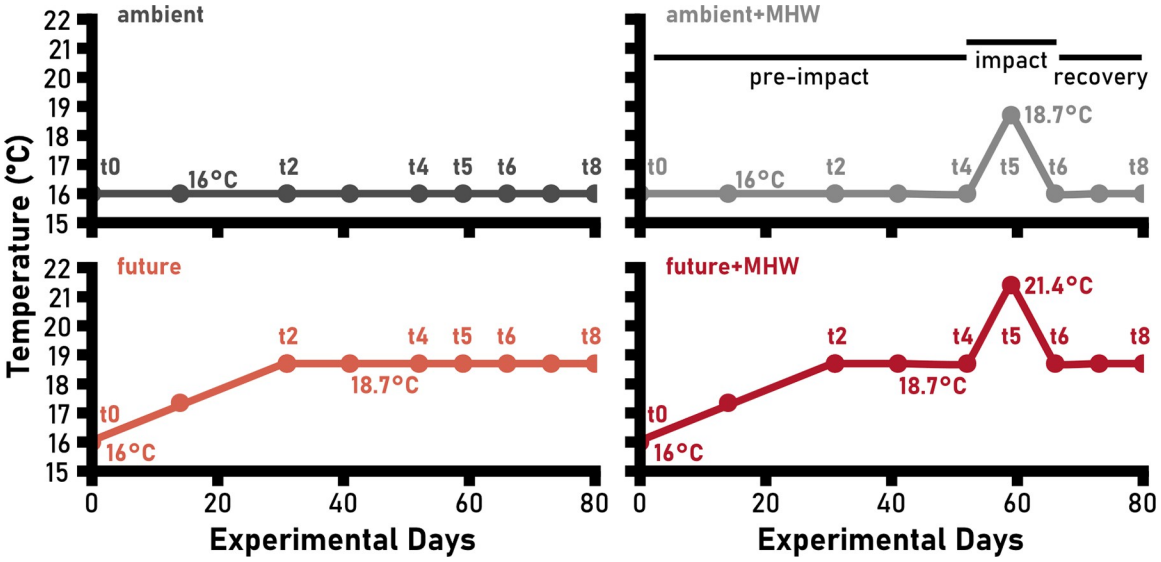

Fig 1. Temperature profile over the course of the experiment in the four treatments (dark grey = ambient; light grey = ambient +MHW; coral = future; dark red = future+MHW). Dots indicate the different timepoints (t) where various measurements were conducted (for further details see specific sections). Horizontal bars indicate different experimental phases (pre-impact t0–t4, impact t4–t6 and recovery period t6–t8).

https://doi.org/10.1371/journal.pclm.0000092.g001

MHWs in the region (S3 Fig). Each treatment was replicated at the tank level twelve times for a total of 48 experimental tanks (S4 Fig). Six experimental tanks from one treatment (~4 L each; 17.5 cm W x 23 cm L x 12 cm H) were organised together in one 60 L water bath (56 cm W x 76 cm L x 18.5 cm H). Thus, a total of eight water baths (two *per* treatment) were used to accommodate all the experimental tanks. The water baths themselves were distributed over two shelf levels due to logistical constraints. These were later treated in our analysis as random factors (see further below).

2.4 Experimental conditions

2.4.1 Seawater supply. The seawater used for the experiment was pumped directly from the shore in front of the laboratory facilities, sand-filtered (mesh size 10 μm) and then fed into our flow-through setup. Seawater was first passed through aquarium chillers to decrease temperature variability. Chilled water was collected in two intermediate tanks (one *per* shelf level with ~60 L in each; 56 cm W x 76 cm L x 18.5 cm H) and pumped from there into the header tanks (~20 L in each; 30 cm W x 25 cm L x 38 cm H) using submersible pumps (Jeboa DC-650, 200 L h^{-1}). There were a total of eight header tanks, and one header tank supplied each of six experimental tanks with 80 mL seawater *per* minute. These were equally distributed over two neighbouring water baths (three *per* water bath). Header tanks contained one pump (Jeboa DC-650, 650 L h^{-1}) for strong water mixing.

2.4.2 Temperature control. Intermediate tanks that collected chilled seawater (see Section 2.4.1) also contained three submersible 300 W heaters that, together with the aquarium chiller, allowed a reduction of the natural temperature variability and the creation of a baseline temperature (14.5–15˚C). Temperature in the individual water baths was controlled using two submersible 300 W titanium heaters. All chillers and heaters were connected to an aquarium control system (AquaController, Neptune systems, USA) that turned the individual units on or off at set points when required. Temperature was measured using temperature probes that were connected to the control systems and placed in each water bath. Pumps (Jeboa DC-650, 650 L h^{-1}) placed in each water bath ensured good mixing of water within the water bath to enhance temperature control. Smaller jet pumps placed in each experimental tank were used to create sufficient horizontal water motion (Hailea BT100, 150 L h^{-1}) and to aid pH and temperature control in the tanks. Temperature in the experimental tanks was checked at regular intervals (results see S2 Table) and daily variability in the treatments did not exceed ±0.3˚C (see S5 Fig), keeping in mind that some level of daily and day-to-day variability occurs at our field sites (see S7 Fig).

2.4.3 Seawater carbonate chemistry. Seawater pH and total alkalinity (A_T) were measured in each header tank and in randomly selected experimental tanks of each water bath every two weeks to assess long- and short-term variability (for results see S3 Table and S6 Fig). The pH was measured using a pH meter (HQ40D equipped with IntelliCal PHC101 probe, Hach Company, Loveland, USA) calibrated on the total scale using Tris/HCl buffers (following [56]). A_T was calculated with a modified Gran function [56]. Regular titrations (AS-ALK2, Apollo SciTech, USA) of certified reference material (CRM, Batch 176 provided by A.G. Dickson lab) yielded A_T values within ± 6 μmol kg^{-1}. Seawater carbonate chemistry was calculated with the "seacarb" package running in R [57].

2.4.4 Light. Light was provided by 72 W light emitting diode (LED) panels (Zeus 70, Shenzhen Ledzeal Green Lighting Co., Ltd, Shenzhen, China) mounted over each water bath. The LEDs were designed to mimic a natural coastal underwater light spectrum (for details see [52]) and followed a natural diel cycle. Irradiance increased gradually in two steps (6:30–9:30 and 9:30–12:30) to reach maximum levels in the afternoon (12:30–16:30 h) and decreased

again in two steps (16:30–18:30 h and 18:30–20:30 h). Light levels were set to a peak irradiance of 80 μmol photons m^{-2} s^{-1} PAR (daily dose 2.3 mol photons m^{-2} d^{-1} PAR) in all tanks, as these organisms encounter this frequently in their natural environment (see [52]). Maintenance of the light level in the individual tanks was achieved by covering them with coated metal mesh and shade cloth. Light levels were checked regularly using an underwater PAR meter (Apogee MQ-510, Apogee Instruments, Inc., North Logan, USA).

2.5 Physiological measurements

2.5.1 Photosynthetic efficiency. The Fv/Fm of each individual was measured at all timepoints (t0–t8) (Fig 1) using a Pulse Amplitude Modulated chlorophyll fluorometer (Diving PAM/R, Heinz Walz GmbH, Effeltrich, Germany) [58, 59]. Settings were adjusted for each species to ensure reliable results (saturation light intensity = 8 for *Corallina* complex. 1, *Corallina* complex. 2 and *Corallina/Arthrocardia* "robust" and 7 for *Phymtolithopsis complex*; gain = 1; damping = 2; measuring light intensity = 1; saturation pulse width = 0.8). Individuals were dark-adapted prior to each measurement for at least 30 min. Thus, measurements were only taken after 9 pm and if Fo >120. The distance between the PAM fibre optic and the samples was standardised to 2 mm using pre-set PAM clips.

Individual measurements taken at t0, t2 and t4 were averaged to obtain a single value for Fv/Fm for the pre-impact/baseline period. This value was subtracted from the respective value obtained during the impact phase (t5 only) and the recovery period (average of Fv/Fm from t6 and t8), thus anchoring them to a baseline. Fv/Fm standardised in this way will be reported here.

2.5.2 Light curves. Effective photosynthetic capacity and light acclimation state were assessed at t4, t6 and t8 (Fig 1) using the PAM's rapid light curve (RLC) function. Relative electron transport rates (rETR) were obtained at noon from five individuals of each species in each treatment. Individuals were exposed for 20 s to nine increasing light steps ranging from 0 to 213 μmol photons m^{-2} s^{-1} PAR. Here too, distance between samples and the PAM fibre optic was set to 2 mm using pre-set PAM clips. Non-linear models were then fitted to the data based on least-square error calculations, to determine maximum relative electron transport rate ($rETR_{max}$), light use efficiency (α or initial curve slope) and minimum saturation intensity (E_k) [58, 59].

2.5.3 Pigment content. Pigment content was determined from samples taken at t5 and t8 (Fig 1). Therefore, five individuals of each species in each treatment were taken out of the experiment at each timepoint to obtain fresh tissue samples. An additional 10 individuals were removed at t6 (MHW treatments only), but these were not analysed (for more details regarding sample removal see S1 Table). Red pigments (phycocyanin and phycoerythrin) were extracted using phosphate buffer (after [60]). Chlorophyll *a* (Chl *a*) content was extracted using ethanol (after [61]). Pigment absorbance was measured with a spectrophotometer (Evolution 300, Thermo-Fisher Scientific, Loughborough, UK) and pigment content was calculated after [60] for red pigments and [61] for chlorophyll pigments.

2.5.4 Mean-net calcification. Mean-net calcification rates were quantified using the buoyant weight technique [62]. Organisms were weighed at the start of the experiment (t0), the end of the acclimation phase (t4), the end of the impact phase (t6) and the end of the recovery phase (t8). The difference in weight between individual timepoints was converted into dry weight of calcite and used to calculate net calcification for the different experimental periods (t0 and t4 = pre-impact/baseline period; t4 and t6 = impact period; t6 and t8 = recovery period). Net weight changes were transformed into calcification rates (mg $CaCO_3$ cm^{-2} d^{-1}) by normalising for time (in days) and surface area (in cm^2, for details see Section 2.6). To ensure the correct calculation of calcification rate for the geniculate coralline algae, the weight of the epoxy bases had to be subtracted. Therefore, bases were weighed after the experiment

following the complete removal of the algae, and the obtained weight was subtracted from the individual sample weight from each timepoint.

Individual calcification rates for the pre-impact/baseline period (t0–t4) were subtracted from the respective rates obtained during the impact (t4–t6) and the recovery period (t6–t8), thus anchoring them to a baseline. Calcification rates standardised in this way will be reported here.

2.5.5 Raman spectroscopy. Confocal Raman spectroscopy was used to determine sample minerology and proxies that follow calcifying fluid saturation state (Ω_{CF}) in coral and likely do so in coralline algae also [63, 64]. Measurements were conducted with a Horiba Jobin-Yvon Labram HR Raman spectroscope (Horiba France SAS, Longjumeau, France) using a green 514 nm Ar-ion laser following DeCarlo et al. [65] (further details regarding the configuration see [52]). Therefore, a total of 20 individuals *per* species (five *per* treatment) were taken out of the experiment, bleached, and analysed at the timepoints t5 (peak of impact phase) and t8 (end of recovery period). An additional 10 individuals were removed at t6 (MHW treatments only), but these were not analysed (for more details regarding sample removal see S1 Table). For each individual, three spectra (integration 4x3s) were obtained (one spectrum each from surface cells located on three different growth margins). Low quality or contaminated spectra were excluded from the analysis. The minerology of the sample was determined by the presence and shape of two peaks. The ν1 peak (1,085–1,090 cm^{-1}) which is indicative for $CaCO_3$ and the shape of the ν4 peak (700–720 cm^{-1}) which indicates presence of aragonite (double peak) or calcite (single peak) [66]. Full width at half maximum intensity (FWHM) and position of the ν1 peak were used to determine Mg content and to approximate calcifying fluid Ω [65]. Abiogenic calibrations of Perrin et al. [67] were used to estimate mol% Mg after correcting for the divergence of the Si wavenumber obtained in this study and that reported by Perrin et al. [67]. The calculated Mg content was also used to account for the effects of high Mg content on FWHM. Residual ν1 FWHM was considered a proxy for calcifying fluid Ω of high-Mg calcite.

2.6 Determination of surface area

Surface area of crustose species (*Phymatolithopsis* complex) was determined using the aluminium foil method [68]. The surface area of geniculate coralline algae (*Corallina* complex 1, *Corallina* complex 2, *Corallina/Arthrocardia* "robust") was determined by establishment of a relationship between dry weight and surface area (for details see [52]).

2.7 Statistical analysis

The effect of temperature and the heatwave on all measured parameters was examined using linear mixed effect models (R package "lme4") whenever possible. Temperature, MHW and their interaction was used as a fixed, water bath and header tank as random effects. The assumptions of normality and equality of variance were evaluated through graphical analyses of residuals using the R software package "sjPlot". Treatment effects were determined using one-way ANOVAs with p-values calculated using "lmerTest". Proportions of the variation (R^2) explained by the full models were calculated using the package "MuMin". The data underlying this study are available at Dryad [69].

3 Results

3.1 Photosynthetic efficiency

Standardised photosynthetic efficiency (Fv/Fm) in the different treatments during the impact (Fig 2A) and the recovery phase (Fig 2B) were not significantly affected by OW, the MHW or their interaction in any of the species (S4 and S5 Tables; for pre-impact Fv/Fm see S8 Fig).

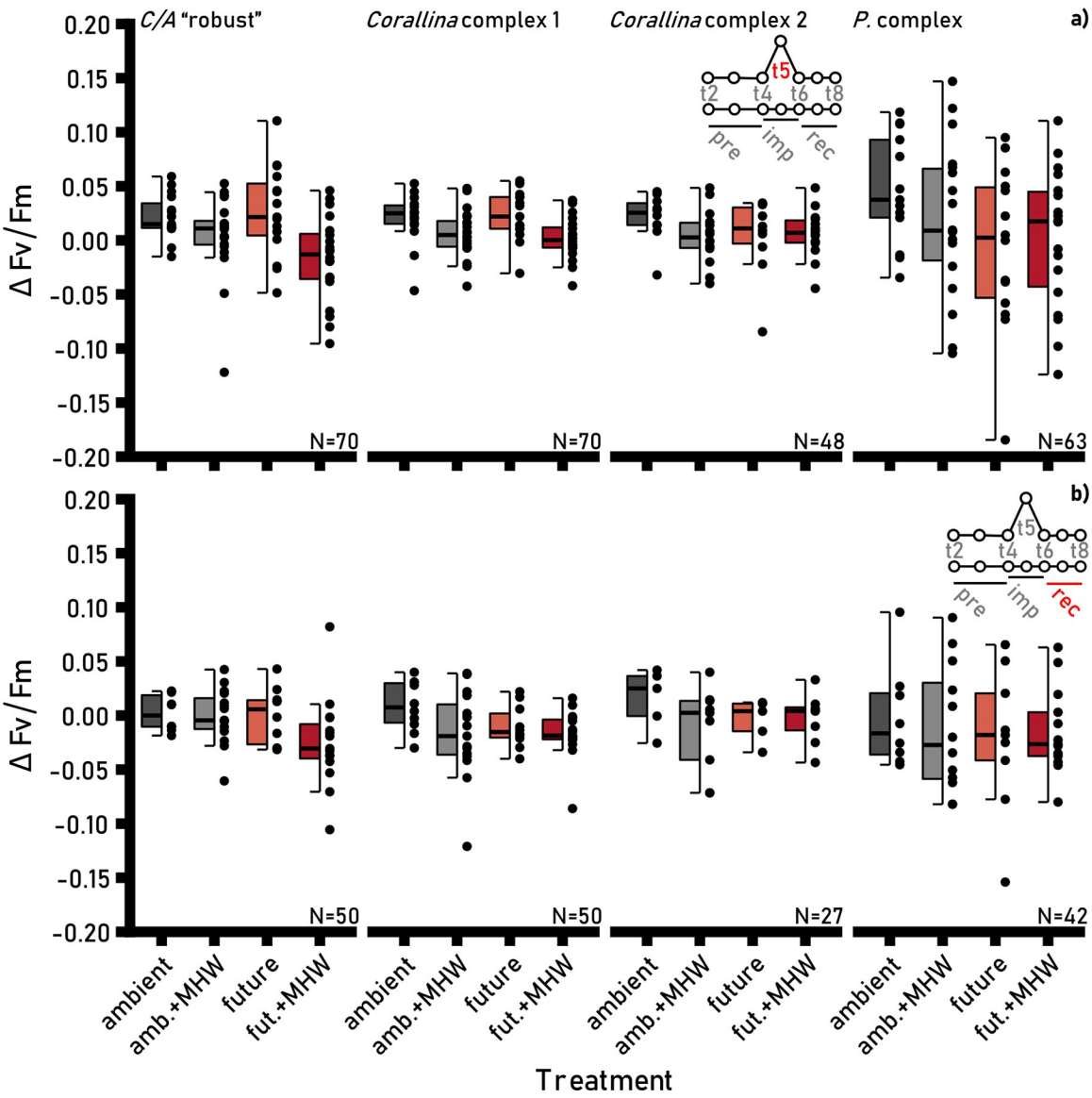

Fig 2. Standardised photosynthetic efficiency (Fv/Fm) of *Corallina*/*Arthrocardia* "robust", *Corallina* complex 1, *Corallina* complex 2 and *Phymatolithopsis* complex during the impact (a) and the recovery (b) phase in the different treatments. Points show individual values. Solid line indicates the median, box shows the interquartile range (IQR) and the whiskers are 1.5×IQR. Colours indicate treatments (dark-grey = ambient [16˚C]; light-grey = amb.+MHW [16˚C+2.7˚C at t5], coral = future [18.7˚C], dark-red = fut.+MHW [18.7˚C+2.7˚C at t5]). "Pre", "imp" and "rec" denotes the three experimental phases (pre-impact, impact and recovery). Note: standardisation was achieved by subtraction of the respective Fv/Fm values from the pre-impact phase. Thus, 0 = no change, <0 = lower efficiency and >0 = higher efficiency.

https://doi.org/10.1371/journal.pclm.0000092.g002

3.2 Rapid light curves

Maximum relative electron transport ($rETR_{max}$; Fig 3 and S6–S8 Tables), light-use efficiency (initial slope of the curve or α; S9–S11 Tables and S9 Fig) and maximum saturation intensity (E_k; S12–S14 Tables and S10 Fig) were not significantly affected by the different temperature regimes for any species at any timepoint (pre-impact (t4); immediately after the impact phase (t6) and the end of the recovery phase (t8)).

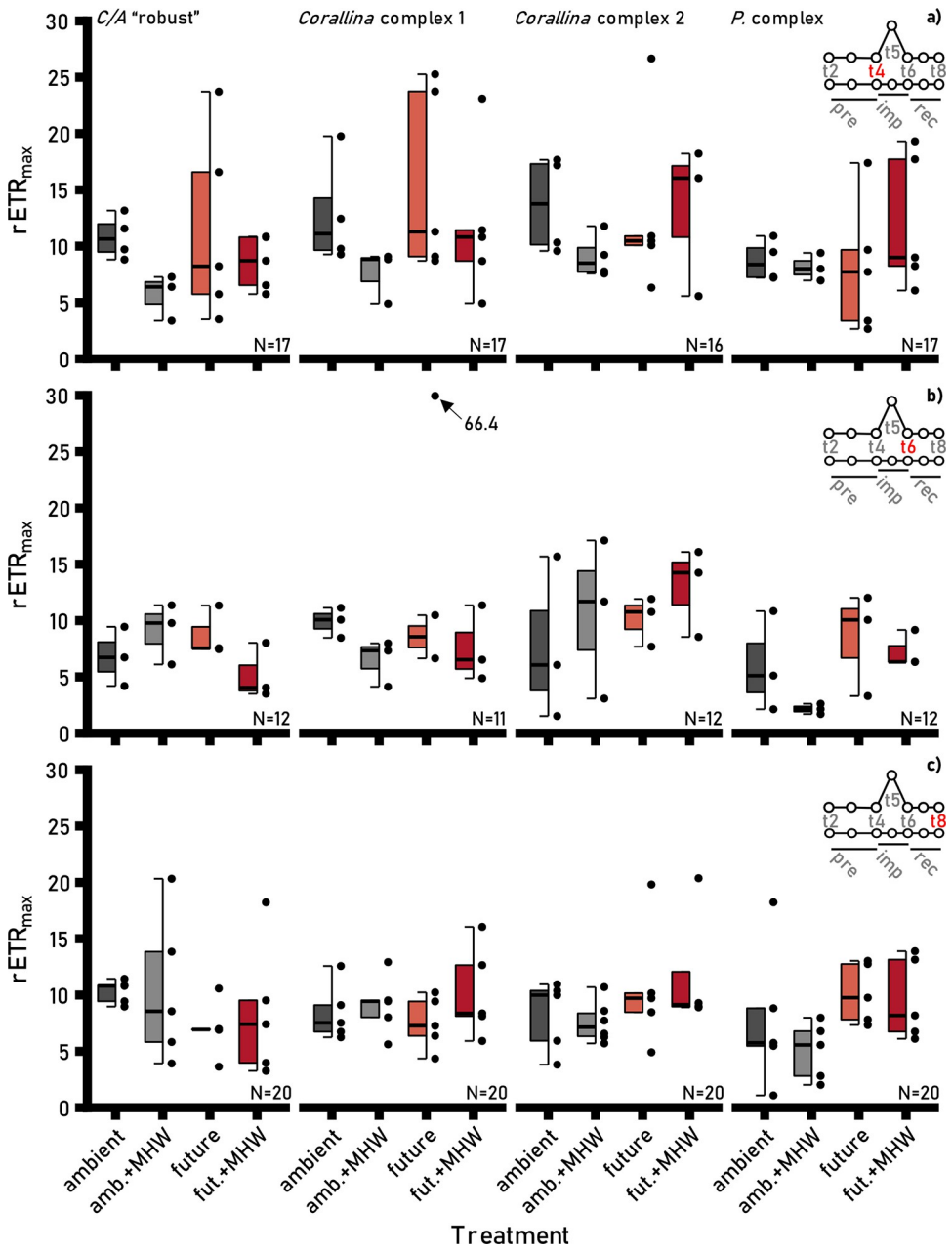

Fig 3. Maximum relative electron transport ($rETR_{max}$) in *Corallina*/*Arthrocardia* "robust", *Corallina* complex 1, *Corallina* complex 2 and *Phymatolithopsis* complex before the impact phase (t4) (a), immediately after the impact phase (t6) (b) and at the end of the recovery phase at t8 (c). Points show individual values. Solid line indicates the median, box shows the interquartile range (IQR) and the whiskers are 1.5×IQR. Colours indicate treatments (dark-grey = ambient [16˚C]; light-grey = amb.+MHW [16˚C+2.7˚C at t5], coral = future [18.7˚C], dark-red = fut.+MHW [18.7˚C+2.7˚C at t5]). "Pre", "imp" and "rec" denotes the three experimental phases (pre-impact, impact and recovery).

https://doi.org/10.1371/journal.pclm.0000092.g003

3.3 Photosynthetic pigment content

3.3.1 Chlorophyll *a*. Chlorophyll *a* (Chl *a*) content was significantly affected during the impact phase (t5; Fig 4A and S15 Table) by OW, the MHW and their interaction only in *Corallina* complex 2. In this species, Chl *a* content decreased as a result of OW ($p < 0.001$) and the

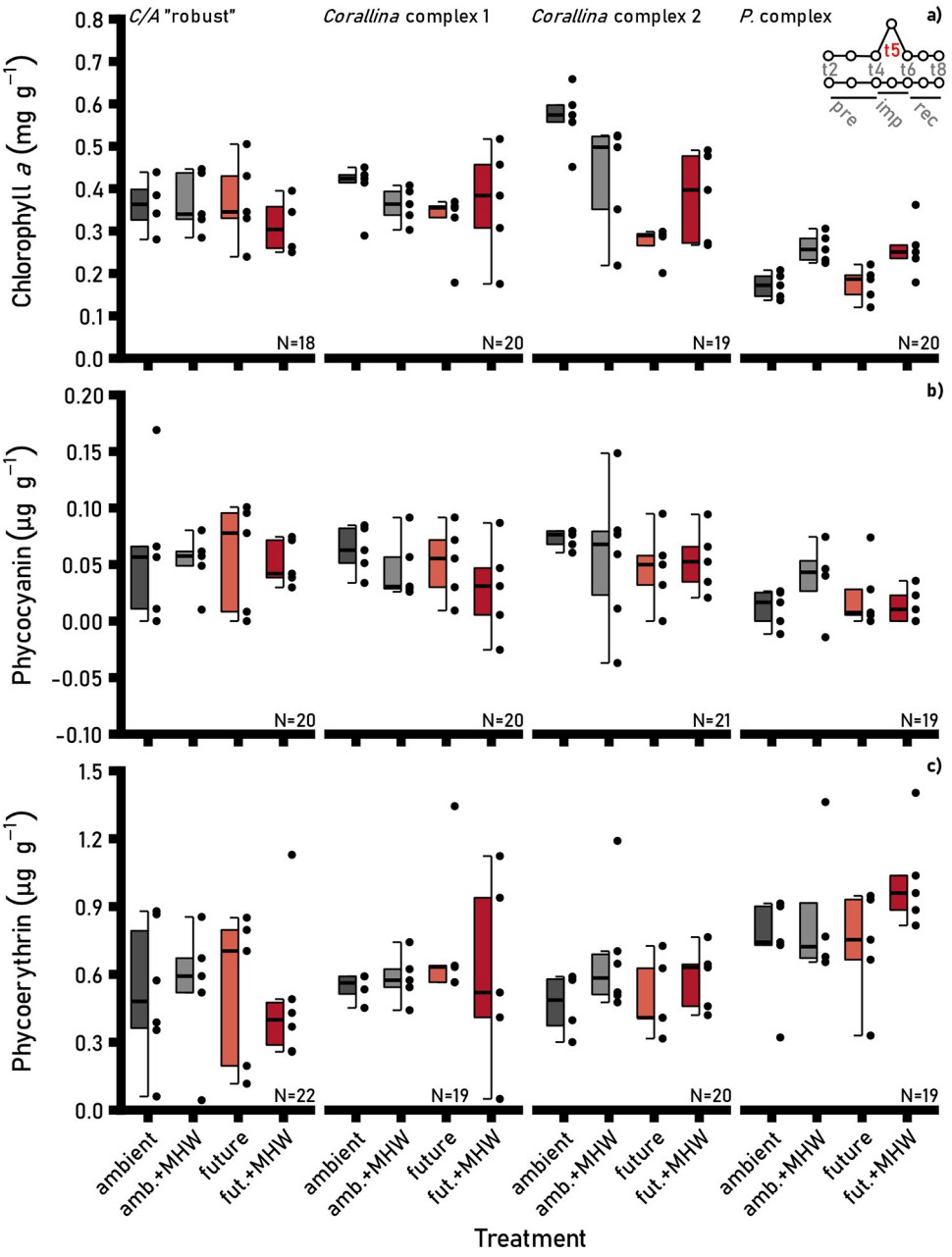

Fig 4. Chlorophyll *a* (a), phycocyanin (b) and phycoerythrin (c) content in *Corallina*/*Arthrocardia* "robust", *Corallina* complex 1, *Corallina* complex 2 and *Phymatolithopsis* complex during the impact phase (t5). Points show individual values. Solid line indicates the median, box shows the interquartile range (IQR) and the whiskers are 1.5×IQR. Colours indicate treatments (dark-grey = ambient [16˚C]; light-grey = amb.+MHW [16˚C+2.7˚C at t5], coral = future [18.7˚C], dark-red = fut.+MHW [18.7˚C+2.7˚C at t5]). "Pre", "imp" and "rec" denotes the three experimental phases (pre-impact, impact and recovery).

https://doi.org/10.1371/journal.pclm.0000092.g004

MHW (p = 0.007), while the interaction between the two factors had a positive impact (p = 0.008).

At the end of the recovery period (t8; S16 Table), Chl *a* content was significantly affected by the treatments only in *Corallina/Arthrocardia "robust"*. In this species, Chl *a* content was significantly lower under OW (p = 0.008).

3.3.2 Phycocyanin. Phycocyanin content was not affected by OW, MHW or their interaction during the impact phase (t5; Fig 4B) in any of the species (S17 Table).

At the end of the recovery phase (t8; S18 Table), phycocyanin levels were significantly higher under OW in *Corallina* complex 2 ($p = 0.045$).

3.3.3 Phycoerythrin. Phycoerythrin content was not significantly affected by OW, MHW or their interaction during the impact phase (t5; Fig 4C) in any of the species (S19 Table).

Similarly, there was no significant difference in phycoerythrin content in any of the species at the end of the recovery period (t8; S20 Table).

3.4 Mean-net calcification

Standardised calcification rates during the impact phase (t4–t6) (Fig 5A) were significantly affected by OW, MHW and their interaction, but only in *Corallina/Arthrocardia* "robust" (S21 Table). In this species, the decline in calcification rate was significantly greater in the ambient temperature treatments (ambient and amb.+MHW) compared to the future temperature treatments (future and fut.+MHW) ($p = 0.039$).

Respective calcification rate during the recovery phase (t6–t8) (Fig 5B and S22 Table) was not significantly affected by OW, MHW and their interaction in any species.

3.5 Geochemistry

3.5.1 Magnesium content. Skeletal magnesium content (% Mg) was significantly affected by OW, the MHW and their interaction during the impact phase (t5; Fig 6A) in *Phymatolithopsis* complex only (S23 Table). In *Phymatolithopsis complex*, % Mg increased significantly due to OW ($p<0.001$), the MHW ($p<0.001$) and the interaction of the two factors ($p < 0.001$). At the end of the recovery phase (t8; S24 Table), % Mg was not affected by any treatment in any of the species.

3.5.2 Residual FWHM. FWHM was significantly affected by the treatments during the impact phase (t5; Fig 6B) only in *Phymatolithopsis complex* (S25 Table). In this species, FWHM was significantly lower at higher temperatures ($p = 0.033$). FWHM at the end of the recovery phase (t8; S26 Table) was not affected by any of the treatments in any of the species.

4 Discussion

4.1 Impact of heat-stress on coralline algal photo-physiology

This study revealed the tolerance of temperate coralline algae to low and moderate heat stress that corresponds to realistic present day and future temperature scenarios. This is contrary to our initial expectations, but generally supported by the findings of three single-species studies from the Mediterranean and the Atlantic [70–72]. The displayed thermo-tolerance is likely linked to the photosynthetic apparatus, which continued to function under heat stress. Photosynthesis is a fundamental yet complex physiological process that is highly sensitive to environmental stress [73]. Upon exposure to adverse abiotic conditions, photosynthetic performance declines rapidly and often well before other physiological processes are impaired [74]. This is readily observable in more intensively studied taxa, including many species of kelp [38, 39], corals [75–77], and higher plants [78, 79], when temperatures approach and exceed (upper) thermal tolerance thresholds. Therefore, we initially expected to see similar patterns in coralline algae, since they were grown far above their maximum summer temperatures, a threshold that has been found to be significant and associated with adverse impacts in many taxa, such as corals [80]. However, photosynthetic efficiency (Fv/Fm) and all other fluorescence parameters ($rETR_{max}$, α, E_k) were not significantly affected by acute or chronic heat

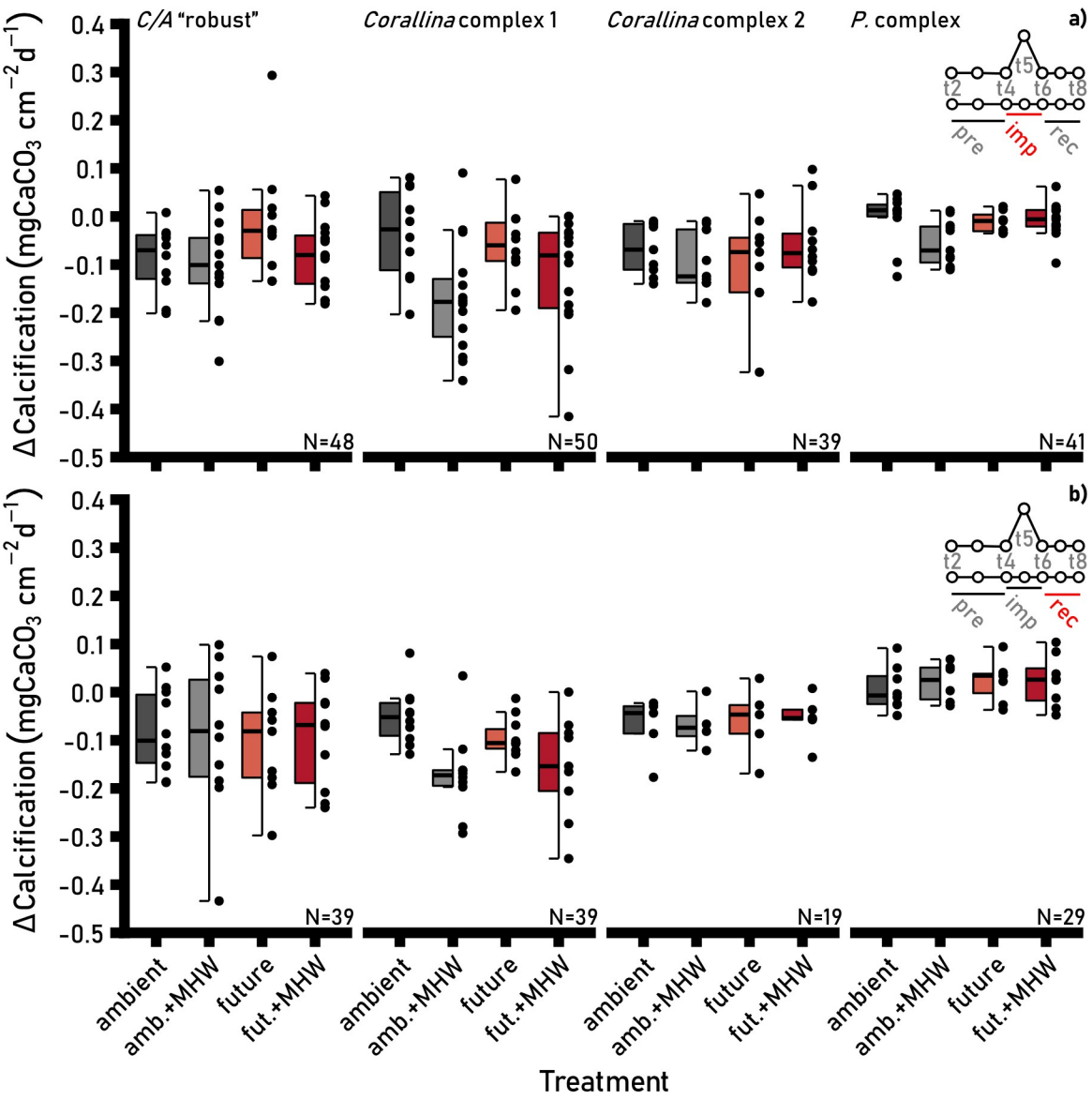

Fig 5. Standardised calcification rates ($mgCaCO_3$ cm^{-2} d^{-1}) of *Corallina*/*Arthrocardia* "robust", *Corallina* complex 1, *Corallina* complex 2 and *Phymatolithopsis* complex during the impact (a) and the recovery (b) phase in the different treatments. Points show individual values. Solid line indicates the median, box shows the interquartile range (IQR) and the whiskers are 1.5×IQR. Colours indicate treatments (dark-grey = ambient [16˚C]; light-grey = amb.+MHW [16˚C+2.7˚C at t5], coral = future [18.7˚C], dark-red = fut.+MHW [18.7˚C+2.7˚C at t5]). "Pre", "imp" and "rec" denotes the three experimental phases (pre-impact, impact and recovery). Note: standardisation was achieved by subtraction of the respective calcification rates from the pre-impact phase. Thus, 0 = no change, <0 = slower calcification and >0 = faster calcification.

https://doi.org/10.1371/journal.pclm.0000092.g005

stress in any of the four morpho-types, indicating tolerance to these changes in temperature. The changes we observed in these parameters and in pigment content appeared to be largely driven by biological and/or technical variability and (if at all) only weakly by temperature, since (statistically significant) variations appeared to be rather sporadic and contradictory at times. In *Corallina* complex 2 for example, chlorophyll *a* content during the impact phase decreased due to OW and the MHW but increased in the treatment where the interactive effects of both were assessed. Moreover, phycocyanin content, generally unaffected, increased

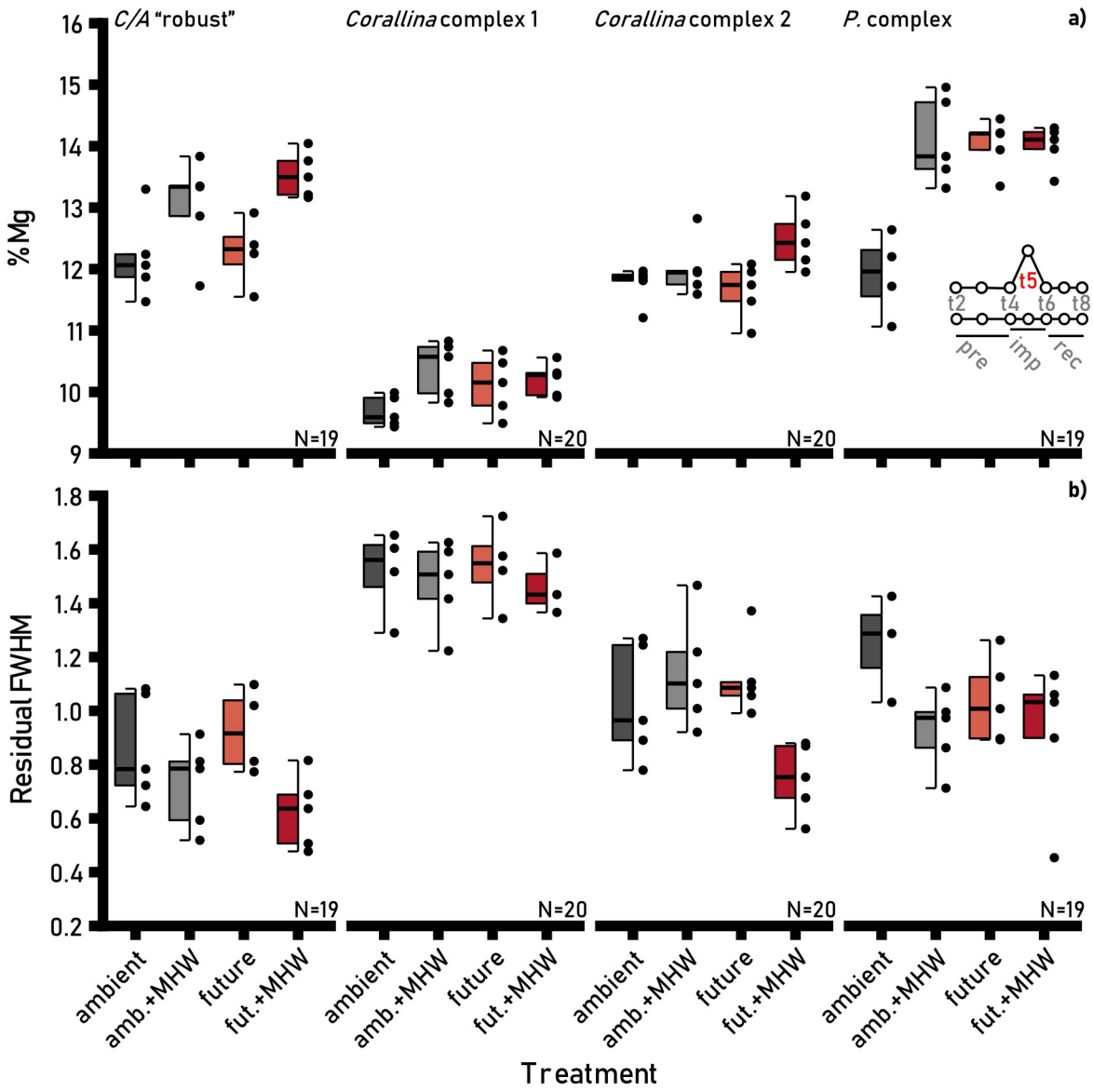

Fig 6. Skeletal magnesium content (a) and residual FWHM (proxy for Ω_{CF}) (b) of *Corallina*/*Arthrocardia* "robust", *Corallina* complex 1, *Corallina* complex 2 and *Phymatolithopsis* complex during the impact phase at t5. Points show individual values. Solid line indicates the median, box shows the interquartile range (IQR) and the whiskers are 1.5×IQR. Colours indicate treatments (dark-grey = ambient [16˚C]; light-grey = amb.+MHW [16˚C+2.7˚C at t5], coral = future [18.7˚C], dark-red = fut.+MHW [18.7˚C+2.7˚C at t5]). "Pre", "imp" and "rec" denotes the three experimental phases (pre-impact, impact and recovery).

https://doi.org/10.1371/journal.pclm.0000092.g006

during the same period in this species in the OW treatment. Furthermore, the magnitude of variation in the physiological parameters was extremely small compared to thermosensitive taxa [81] and thus of seemingly limited physiological significance. Collectively, these results suggest a high thermo-tolerance.

4.2 Impacts of elevated temperatures on calcification and minerology

Calcification physiology was largely unaffected by heat stress. We hypothesised that calcification rates would decline due to heat stress, reflecting knock-on impacts from heat-induced photoinhibition. However, the hypothesized heat-induced photoinhibition did not occur here.

A significant effect of temperature on standardised calcification rates was only detected once, in *Corallina/Arthrocardia* "robust" during the impact phase. This effect was positive, however. Our results are thus generally consistent with the findings of a recent meta-analysis [27] that assessed the effects of temperature on coralline algal calcification. The analysis concluded that a mean negative impact on coralline algal calcification only manifests itself at temperatures of about 5.2˚C above ambient conditions. The relative robustness of this process could be attributed to the fact that calcium carbonate ($CaCO_3$) precipitation is thermodynamically favoured at higher temperatures [82–84]. Additionally, until upper thermal thresholds are reached, increasing temperatures tend to enhance metabolic processes [85]. Based on our results, we suggest that this is also linked to the thermostability of coralline algal photosynthesis that allows continued calcification and enhances overall tolerance. This is supported and complemented by the findings of three other studies that also report limited to no effect of OW or MHWs on coralline algal physiology [70–72, 86]. Together, this implies the resilience of most coralline algae to short- and long-term heat stress.

Magnesium incorporation (Mg) and the internal calcium carbonate saturation state ($\Omega_{CF,}$ approximated using FWHM) were also principally unaffected by elevated temperature. In hindsight, stability is logical for FWHM, given the lack of impacts on photo-physiology. This lack of an effect on photo-physiology likely allowed the maintenance of a stable internal carbonate chemistry which in turn underpinned steady calcification rates [87]. However, we note that, while stable FWHM could indicate the maintenance of a favourable internal carbonate chemistry (i.e., Ω_{CF}), further calibrations are required for the correct correlation of the two parameters [63]. The lack of a detectable temperature signal in the Mg content was somewhat surprising. The incorporation of Mg into the calcite lattice is favoured at higher temperatures [88]. In field samples, Mg content is thus generally highest in summer and lowest in winter with a relationship of ~1 mol% *per* ˚C [88–90]. In our study species, this relationship was much lower (0.1 to 0.4 mol% *per* ˚C) which reemphasises the need for species- and location-specific proxy calibrations [91]. Here, this is likely related to the rate of calcification. Faster calcification is known to increase Mg% irrespective of temperature [52, 92]. Exposure to more favourable light conditions, for example, triggers faster calcification and the increased incorporation of Mg, likely due to the depletion of the internal calcium pool [52]. Thus, it is known that Mg bands in field samples also represent periods of fast (summer) and slow (winter) calcification, with other complex drivers of Mg content usually playing lesser roles [93]. This means that Mg bands incorporate both biology (e.g., more favourable growth conditions in summer) and chemistry (e.g., endothermic substitution of Mg in calcite). In our experiment, calcification rates were stable and seemingly unaffected by temperature. Thus, we only observed a weak "chemical temperature" effect. However, there were exceptions, such as the pronounced increase of Mg in *Phymatolithopsis* complex in the OW and MHW treatments. Yet, in these treatments, calcification rates increased after the impact phase, supporting the hypothesis that Mg is controlled by calcification rate and temperature.

4.3 Ecology of coralline algae in a warming ocean and indirect effects

The tolerance of coralline algae to OW and MHWs displayed here and elsewhere [27, 70–72] suggests that coralline algae are likely to play their ecological roles in a warming ocean (other outcomes of climate change notwithstanding, e.g. ocean acidification or altered biotic interactions). In the tropics, this could mean that coralline algae take up space formerly occupied by corals and thus play a larger role in supporting existing reef structures [11]. Conversely, tropical coralline algae tend to have narrow thermal tolerances which may increase their susceptibility to OW and MHWs [19, 70] and thus diminish their ability to support reef frameworks in

the future. However, the thermal sensitivity of taxa with narrow thermal windows has not been examined experimentally. Additionally, such algal dominated reefs would suffer from a decline in structural complexity and the profound alteration of ecosystem functioning [94].

Coralline algae from temperate regions tend to have broader thermal windows and are therefore arguably more robust to heat stress than tropical ones. However, the impacts of OW and MHWs could be more strongly felt in temperate kelp forest communities. Kelps and fucoids are highly susceptible to OW and MHWs and the loss of canopy-forming brown algae has a strong impact on the understory coralline algal community. In particular, while coralline cover tends to increase, community diversity decreases [95]. Thus, taxa that rely on (heat-sensitive) canopy species are likely to be strongly impacted by OW and MHW irrespective of their own thermo-sensitivity. On the other hand, coralline taxa that do not depend on kelp species, or those that rely on canopy species expanding their range, might profit. Yet, there are many unknowns. Manifestation of heat stress ultimately depends on duration, intensity and rate of the temperature increase [96], but the individual and interactive impact of these factors is unknown. This also applies to impacts of OW and MHWs on early life-stages of coralline algae. In addition, the oceans are not only warming but also pH is decreasing, which is likely the greatest threat to coralline algae [20]. The interactions of ocean warming and acidification seem mostly additive [20], but interactions of OA with heatwaves have not been examined so far. Thus, large uncertainties remain about the fate of coralline algae in a future ocean.

4.4 Potential physiological underpinnings for the thermo-tolerance of coralline algae

The carbon-fixing enzyme (ribulose 1,5-bisphosphate carboxylase/oxygenase or Rubisco) of coralline algae has a high specificity towards CO_2 which could provide thermo-tolerance. The (re-)activation of Rubisco is considered the primary site of thermal damage in photoautotrophs due to the heat-induced inactivation of Rubisco activase [97–99]. It is tempting to speculate that coralline algal activases are more thermostable than those found in corals and kelp. While certainly possible, there is no information available about activase systems and the thermostability of these enzymes in marine macroalgae, which represents a crucial knowledge gap. However, the thermo-tolerance displayed by coralline algae could be related to their possession of type ID Rubisco [100]. The red-algal Rubisco (Type ID) is widely reported to have a very high substrate specificity (use of CO_2 over O_2 or $S_{c/o}$) [100–103]. Type ID specificity can be twice as high as in Type IB (land plants) and over four times higher than Type II (dinoflagellates such as Symbiodiniaceae) [101, 102, 104]. High $S_{c/o}$ Rubiscos increase photosynthetic efficiency by reducing energetically wasteful pathways (photorespiration) [105]. These properties seem to have been selected for in plants and algae from more extreme and hot environments, and are likely to bolster resilience to global warming in terrestrial photoautotrophs [103, 106]. However, we lack the information about the kinetics of Rubisco in coralline algae and other micro- and macroalgae from different habitats and phylogenetic groups to credibly link Rubisco properties with thermo-tolerance. Closing this knowledge gap might help to understand and predict thermal sensitivities in marine algae.

Coralline algal thermo-tolerance might also be related to the ultrastructure of their chloroplast and their light harvesting complexes (LHC). The main LHC of red algae (Rhodophyta) and cyanobacteria are the so-called phycobilisomes (PBS), which are located on the stroma side of the thylakoid membrane [107]. In all other photoautotrophs, LHCs are embedded in the thylakoid membrane, where they form tight stacks (threefold in dinoflagellates and brown algae; true grana in higher plants and some green algae) [108, 109]. These stacks are interconnected by unstacked membranes which contain mostly photosystem I (PSI) and associated

LHCs (LHCI), while PSII (and LHCII) is located mainly in stacked regions [110]. This organisation prevents excitation transfer between the photosystems (spillover) and likely provides several other benefits (see reviews by Chow et al. [111] and Anderson et al. [110]). Yet, it also creates problems. Macromolecular crowding in the grana regions impedes processes that require a high degree of molecular mobility [112]. This includes crucial processes such as state transitions, the PSII repair cycle and other photoprotective mechanisms [113]. The molecular mobility required for these processes is achieved by lumenal swelling and the partial or complete destacking of membranes [113–116]. Membrane destacking is indeed observable in higher plants [78, 117, 118] and Symbiodiniaceae [76, 77] as a response to heat and other environmental stresses. However, the loss of membrane structure causes strong and abrupt reductions or even complete cessation of linear electron transport and thus photosynthetic yield (i.e., Fv/Fm) [76, 77], likely due to spillover and increased non-photochemical quenching. Thylakoids of coralline algae are never stacked. Processes requiring molecular mobility can thus be expected to occur faster. Indeed, it appears that repair of PSII in cyanobacteria is faster than in plants [119], as are state transitions, since PBSomes can move on the outside of the thylakoid membrane [120]. Depending on the model [121], the latter might also occur much more gradually and subtly. In addition, modification of proteins (e.g., antenna proteins) and insertion of new proteins could occur faster, since ribosomes can access membranes, so facilitating responses to environmental change. Furthermore, the structural integrity of thylakoids is continuously preserved, which appears to be tightly linked with the ability to tolerate heat and other stresses in corals and plants [76–78, 117, 118].

5 Conclusion

Our results demonstrate the tolerance of four coralline algal morphotypes to ocean warming and marine heatwaves. We attribute this to their photosynthetic apparatus, which was seemingly unaffected by the applied heat stress. Stable photosynthetic efficiency (Fv/Fm) and electron transport rates indicate neither photodamage nor increased non-photochemical quenching from photoprotective mechanisms. Calcification thus also remained quite stable and insensitive to the treatments. Experimental evidence presented here and elsewhere therefore implies that coralline algae are likely to be able to continue to play their important ecological roles in a warming ocean. However, crucial information is lacking. For example, the impact of OW and MHWs on early life stages is not known as is the interaction of these stressors with ocean acidification and changes in light intensity. Little understood is also the role of temperature variability in shaping responses to OW and MHWs. In addition, the scientific community should begin to explore how the duration, intensity, and rate of temperature increase impact the responses to marine heatwaves. Unexplored are also the underlying mechanisms that determine sensitivity to heat stress in coralline algae and other seaweed. Future research should provide this information, to reduce uncertainty regarding the fate of coralline algae and other marine micro- and macrophytes in a warming ocean. Notwithstanding, our results support the emerging picture that coralline algae are more robust to these anthropogenic drivers than other photoautotrophs and foundation species.

Supporting information

S1 Text. Data underlying this study are available at Dryad: https://doi.org/10.5061/dryad.jwstqjqdh.
(TXT)

S1 Fig. Pictures showing the morphology of the four study species/species complexes. Please note the morphological differences between the two *Corallina* morpho-types. *Corallina* complex 2 from the shallow subtidal (<50cm) was smaller and more stunted/compact than *Corallina* complex 1 which was collected slightly deeper (1-2m) (Photos: Erik C. Krieger).
(DOCX)

S2 Fig. Long-term (1st Jan. 1982–31st Dec. 2020) mean sea surface temperature around New Zealand in March. Blue dot indicates position for which local climatology was calculated (see S3 Fig). Plot was created using satellite derived data. Shoreline data was downloaded from http://www.soest.hawaii.edu/pwessel/gshhg/.
(DOCX)

S3 Fig. a) "Lollipop" plot showing marine heat waves (represented by maximum intensities) for Wellington (see S2 Fig). Dashed line indicates the MHW intensity chosen for this experiment (2.7˚C). **b)** Local climatology for Wellington for the period between 1st Jan. 2017 and 1st Jan. 2019. Solid grey line indicates the long-term mean. Temperatures above the 90% climatological average (solid green line) that persisted for over 5 days (= MHW) are highlighted in red. Dashed grey lines indicate the ambient temperature selected (~16˚C) for this experiment that usually occurs at the time of collection in March (NZ late summer/early autumn). Both plots were created using satellite derived daily sea surface temperatures from 1st Jan. 1982 to 31st Dec. 2020 and the R package "heatwaveR".
(DOCX)

S4 Fig. Schematic of the experimental setup. Colour code for treatments will be used in other figures in the remainder of the text.
(DOCX)

S5 Fig. Diel temperature variation in the four treatments (dark-grey = ambient; light-grey = amb.+MHW, coral = future, dark-red = fut.+MHW) measured using temperature loggers. Points indicate individual values (logging interval 5 minutes). Please note: logger data was randomly selected from different days after the impact phase (t6–t8). Drop in temperature in the future treatment due to cleaning activities. During these 25 minutes organisms were kept in a different tank containing warmer water.
(DOCX)

S6 Fig. Diel pH_T variation in the four treatments (dark-grey = ambient; light-grey = amb. +MHW, coral = future, dark-red = fut.+MHW). Points show mean pH_T (±SE) measured over the course of the experiment at different times of the day (n = 88 for each treatment).
(DOCX)

S7 Fig. Temperature variability at the collection site. Dots indicate daily mean temperature. Upper and lower grey bars represent daily temperature maxima and minima.
(DOCX)

S8 Fig. Mean photosynthetic efficiency (Fv/Fm) of *Corallina*/*Arthrocardia* "robust", *Corallina* complex 1, *Corallina* complex 2 and *Phymatolithopsis* complex during the pre-impact phase in the different treatments. Points show individual values. Solid line indicates the median, box shows the interquartile range (IQR) and the whiskers are 1.5×IQR. Colours indicate treatments (dark-grey = ambient [16˚C]; light-grey = amb.+MHW [16˚C+2.7˚C at t5], coral = future [18.7˚C], dark-red = fut.+MHW [18.7˚C+2.7˚C at t5]).
(DOCX)

S9 Fig. Light use efficiency (α) in *Corallina*/*Arthrocardia* "robust", *Corallina* complex 1, *Corallina* complex 2 and *Phymatolithopsis* complex before the impact phase (t4) (a), immediately after the impact phase (t6) (b) and at the end of the recovery phase at t8 (c). Points show individual values. Solid line indicates the median, box shows the interquartile range (IQR) and the whiskers are 1.5×IQR. Colours indicate treatments (dark grey = ambient [16˚C]; light-grey = amb.+MHW [16˚C+2.7˚C at t5], coral = future [18.7˚C], dark-red = fut.+MHW [18.7˚C+2.7˚C at t5]). "Pre", "imp" and "rec" denotes the three experimental phases (pre-impact, impact and recovery).
(DOCX)

S10 Fig. Minimum saturation intensity (E_k) in *Corallina*/*Arthrocardia* "robust", *Corallina* complex 1, *Corallina* complex 2 and *Phymatolithopsis* complex before the impact phase (t4) (a), immediately after the impact phase (t6) (b) and at the end of the recovery phase at t8 (c). Points show individual values. Solid line indicates the median, box shows the interquartile range (IQR) and the whiskers are 1.5×IQR. Colours indicate treatments (dark grey = ambient [16˚C]; light-grey = amb.+MHW [16˚C+2.7˚C at t5], coral = future [18.7˚C], dark-red = fut. +MHW [18.7˚C+2.7˚C at t5]). "Pre", "imp" and "rec" denotes the three experimental phases (pre-impact, impact and recovery).
(DOCX)

S1 Table. Number of replicates for each species-treatment combination in the different experimental periods.
(DOCX)

S2 Table. Mean temperature (±SE) in the treatments during the different experimental periods.
(DOCX)

S3 Table. Mean total alkalinity (A_T) and dissolved inorganic carbon (DIC) measured over the course of the experiment at different times of the day. DIC was calculated from A_T and pH_T. All values are given as μmol kg^{-1} ± SE.
(DOCX)

S4 Table. Standardised photosynthetic efficiency (Fv/Fm) during the impact phase (t4–t6).
(DOCX)

S5 Table. Standardised photosynthetic efficiency (Fv/Fm) during the recovery phase (t6–t8).
(DOCX)

S6 Table. Maximum relative electron transport rates ($rETR_{max}$) at the beginning of the impact phase (t4).
(DOCX)

S7 Table. Maximum relative electron transport rates ($rETR_{max}$) after the impact phase (t6).
(DOCX)

S8 Table. Maximum relative electron transport rates ($rETR_{max}$) at the end of the recovery phase (t8).
(DOCX)

S9 Table. Light use efficiency (alpha or α) at the beginning of the impact phase (t4).
(DOCX)

S10 Table. Light use efficiency (alpha or α) at the end of the impact phase (t6).
(DOCX)

S11 Table. Light use efficiency (alpha or α) at the end of the recovery phase (t8).
(DOCX)

S12 Table. Minimum saturation intensity (E_k) at the beginning of the impact phase (t4).
(DOCX)

S13 Table. Minimum saturation intensity (E_k) at the end of the impact phase (t6).
(DOCX)

S14 Table. Minimum saturation intensity (E_k) at the end of the recovery phase (t8).
(DOCX)

S15 Table. Chlorophyll *a* concentration at the peak of the impact phase (t5).
(DOCX)

S16 Table. Chlorophyll *a* concentration at the end of the recovery phase (t8).
(DOCX)

S17 Table. Phycocyanin concentration at the peak of the impact phase (t5).
(DOCX)

S18 Table. Phycocyanin concentration at the end of the recovery phase (t8).
(DOCX)

S19 Table. Phycoerythrin concentration at the peak of the impact phase (t5).
(DOCX)

S20 Table. Phycoerythrin concentration at the end of the recovery phase (t8).
(DOCX)

S21 Table. Standardised calcification rates during the impact phase (t4–t6).
(DOCX)

S22 Table. Standardised calcification rates during the recovery phase (t6–t8).
(DOCX)

S23 Table. Skeletal magnesium (mol% Mg) at the peak of the impact phase (t5).
(DOCX)

S24 Table. Skeletal magnesium (mol% Mg) at the end of the recovery phase (t8).
(DOCX)

S25 Table. Residual Full Width Half Maximum (FWHM; proxy for calcifying fluid saturation state Ω_{CF}) of the $CaCO_3$ peak at the peak of the impact phase (t5).
(DOCX)

S26 Table. Residual Full Width Half Maximum (FWHM; proxy for calcifying fluid saturation state Ω_{CF}) of the $CaCO_3$ peak at the end of the recovery phase (t8).
(DOCX)

Acknowledgments

We thank R. D'Archino for training in molecular identification.

Author Contributions

Conceptualization: Erik C. Krieger, Aleluia Taise, Wendy A. Nelson, Simon K. Davy, Christopher E. Cornwall.

Data curation: Erik C. Krieger, Aleluia Taise.

Formal analysis: Erik C. Krieger.

Investigation: Erik C. Krieger.

Methodology: Erik C. Krieger, Wendy A. Nelson.

Resources: Johan Grand, Eric Le Ru.

Supervision: Wendy A. Nelson, Simon K. Davy, Christopher E. Cornwall.

Validation: Erik C. Krieger.

Visualization: Erik C. Krieger.

Writing – original draft: Erik C. Krieger.

Writing – review & editing: Aleluia Taise, Wendy A. Nelson, Johan Grand, Eric Le Ru, Simon K. Davy, Christopher E. Cornwall.

References

1. Nelson WA. Calcified macroalgae—critical to coastal ecosystems and vulnerable to change: a review. Mar Freshw Res. 2009; 60: 787. https://doi.org/10.1071/MF08335
2. Bosence DWJ. Coralline algal reef frameworks. J Geol Soc London. 1983; 140: 365–376. https://doi.org/10.1144/gsjgs.140.3.0365
3. Connell SD. The monopolization of understorey habitat by subtidal encrusting coralline algae: A test of the combined effects of canopy-mediated light and sedimentation. Mar Biol. 2003; 142: 1065–1071. https://doi.org/10.1007/s00227-003-1021-z
4. Steneck R. The Ecology of Coralline Algal Crusts: Convergent Patterns and Adaptative Strategies. Annu Rev Ecol Syst. 1986; 17: 273–303. https://doi.org/10.1146/annurev.ecolsys.17.1.273
5. Smale DA, Epstein G, Hughes E, Mogg AOM, Moore PJ. Patterns and drivers of understory macroalgal assemblage structure within subtidal kelp forests. Biodivers Conserv. 2020; 29: 4173–4192. https://doi.org/10.1007/s10531-020-02070-x
6. Barner AK, Hacker SD, Menge BA, Nielsen KJ. The complex net effect of reciprocal interactions and recruitment facilitation maintains an intertidal kelp community. J Ecol. 2016; 104: 33–43. https://doi.org/10.1111/1365-2745.12495
7. Weiss A, Martindale RC. Crustose coralline algae increased framework and diversity on ancient coral reefs. PLoS One. 2017; 12: e0181637. https://doi.org/10.1371/journal.pone.0181637 PMID: 28783733
8. Teichert S, Steinbauer M, Kiessling W. A possible link between coral reef success, crustose coralline algae and the evolution of herbivory. Sci Rep. 2020; 10: 17748. https://doi.org/10.1038/s41598-020-73900-9 PMID: 33082388
9. Björk M, Mohammed SM, Björklund M, Semesi A. Coralline Algae, Important Coral-Reef Builders Threatened by Pollution. Ambio. 1995; 24: 502–505. https://doi.org/10.2307/4314397
10. Littler M, & Littler DS (2013). The nature of crustose coralline algae and their interactions on reefs. Smithsonian Contributions to the Marine Sciences, 39, 199–212.
11. Cornwall CE, Comeau S, Kornder NA, Perry CT, van Hooidonk R, DeCarlo TM, et al. Global declines in coral reef calcium carbonate production under ocean acidification and warming. Proc Natl Acad Sci. 2021; 118: e2015265118. https://doi.org/10.1073/pnas.2015265118 PMID: 33972407
12. Heyward A, Moore C. Benthic habitat characterisation of Montgomery reef: Assessing the distribution and relative abundance of dominant benthic communities. 2009.
13. Ballesteros E. Mediterranean Coralligenous Assemblages. Oceanography and Marine Biology. CRC Press; 2006. pp. 123–195. https://doi.org/10.1201/9781420006391.ch4

14. Riosmena-Rodríguez R., Nelson W., and Aguirre J. (Eds) (2017). Rhodolith/Maërl Beds: A Global Perspective. Switzerland: Springer International Publishing. 368.

15. Le Nohaïc M, Ross CL, Cornwall CE, Comeau S, Lowe R, McCulloch MT, et al. Marine heatwave causes unprecedented regional mass bleaching of thermally resistant corals in northwestern Australia. Sci Rep. 2017; 7: 1–11. https://doi.org/10.1038/s41598-017-14794-y PMID: 29101362

16. Kitamura H, Kitahara S, Koh HB. The induction of larval settlement and metamorphosis of two sea urchins, Pseudocentrotus depressus and *Anthocidaris crassispina*, by free fatty acids extracted from the coralline red alga *Corallina pilulifera*. Mar Biol. 1993; 115: 387–392. https://doi.org/10.1007/BF00349836

17. Pearce CM, Scheibling RE. Effect of macroalgae, microbial films, and conspecifics on the induction of metamorphosis of the green sea urchin *Strongylocentrotus droebachiensis* (Müller). J Exp Mar Bio Ecol. 1991; 147: 147–162. https://doi.org/10.1016/0022-0981(91)90179-Z

18. Morse DE. Flypapers for Coral and Other Planktonic Larvae. Bioscience. 1996; 46: 254–262. https://doi.org/10.2307/1312832

19. Roberts RD, Kaspar HF, Barker RJ. Settlement of abalone (*Haliotis iris*) larvae in response to five species of coralline algae. J Shellfish Res. 2004; 23: 975–987.

20. Cornwall CE, Harvey BP, Comeau S, Cornwall DL, Hall-Spencer JM, Peña V, et al. Understanding coralline algal responses to ocean acidification: Meta-analysis and synthesis. Glob Chang Biol. 2021; 28: 362–374. https://doi.org/10.1111/gcb.15899 PMID: 34689395

21. Guy-Haim T, Silverman J, Raddatz S, Wahl M, Israel A, Rilov G. The carbon turnover response to thermal stress of a dominant coralline alga on the fast warming Levant coast. Limnol Oceanogr. 2016; 61: 1120–1133. https://doi.org/10.1002/lno.10279

22. Tanaka Y, Suzuki A, Sakai K. Effects of elevated seawater temperature and phosphate enrichment on the crustose coralline alga *Porolithon onkodes* (Rhodophyta). Phycol Res. 2017; 65: 51–57. https://doi.org/10.1111/pre.12152

23. Noisette F, Duong G, Six C, Davoult D, Martin S. Effects of elevated pCO_2 on the metabolism of a temperate rhodolith *Lithothamnion corallioides* grown under different temperatures. J Phycol. 2013; 49: 746–757. https://doi.org/10.1111/jpy.12085 PMID: 27007207

24. Comeau S, Carpenter RC, Edmunds PJ. Effects of irradiance on the response of the coral *Acropora pulchra* and the calcifying alga *Hydrolithon reinboldii* to temperature elevation and ocean acidification. J Exp Mar Bio Ecol. 2014; 453: 28–35. https://doi.org/10.1016/j.jembe.2013.12.013

25. Martin S, Cohu S, Vignot C, Zimmerman G, Gattuso JP. One-year experiment on the physiological response of the Mediterranean crustose coralline alga, *Lithophyllum cabiochae*, to elevated *p*CO2 and temperature. Ecol Evol. 2013; 3: 676–693. https://doi.org/10.1002/ece3.475 PMID: 23533024

26. Steller D, Hernandez-Ayón J, Riosmena-Rodríguez R, Cabello-Pasini A. Effect of temperature on photosynthesis, growth and calcification rates of the free-living coralline alga *Lithophyllum margaritae*. Ciencias Mar. 2007; 33: 441–456. https://doi.org/10.7773/cm.v33i4.1255

27. Cornwall CE, Diaz-Pulido G, Comeau S. Impacts of Ocean Warming on Coralline Algal Calcification: Meta-Analysis, Knowledge Gaps, and Key Recommendations for Future Research. Front Mar Sci. 2019; 6: 186. https://doi.org/10.3389/fmars.2019.00186

28. Gleckler PJ, Durack PJ, Stouffer RJ, Johnson GC, Forest CE. Industrial-era global ocean heat uptake doubles in recent decades. Nat Clim Chang. 2016; 6: 394–398. https://doi.org/10.1038/nclimate2915

29. Levitus S, Antonov JI, Boyer TP, Baranova OK, Garcia HE, Locarnini RA, et al. World ocean heat content and thermosteric sea level change (0–2000 m), 1955–2010. Geophys Res Lett. 2012; 39: 1–5. https://doi.org/10.1029/2012GL051106

30. Cheng L, Abraham J, Hausfather Z, Trenberth KE. How fast are the oceans warming? Science. 2019; 363: 128–129. https://doi.org/10.1126/science.aav7619 PMID: 30630919

31. IPCC, 2021: Climate Change 2021: The Physical Science Basis. Contribution of Working Group I to the Sixth Assessment Report of the Intergovernmental Panel on Climate Change [Masson-Delmotte V., P. Zhai A. Pirani S.L. Connors. Péan S. Berger N. Caud Y. Chen L. Goldfarb M.I. Gomis M. Huang K. Leitzell E. Lonnoy J.B.R. Matthews T.K. Maycock T. Waterfield O. Yelekçi R.Yu, and Zhou B. (eds.)]. Cambridge University Press. In Press.

32. Oliver ECJ, Donat MG, Burrows MT, Moore PJ, Smale DA, Alexander L V., et al. Longer and more frequent marine heatwaves over the past century. Nat Commun. 2018; 9: 1324. https://doi.org/10.1038/s41467-018-03732-9 PMID: 29636482

33. Frölicher TL, Fischer EM, Gruber N. Marine heatwaves under global warming. Nature. 2018; 560: 360–364. https://doi.org/10.1038/s41586-018-0383-9 PMID: 30111788

34. Oliver ECJ, Burrows MT, Donat MG, Sen Gupta A, Alexander L V., Perkins-Kirkpatrick SE, et al. Projected Marine Heatwaves in the 21st Century and the Potential for Ecological Impact. Front Mar Sci. 2019; 6: 1–12. https://doi.org/10.3389/fmars.2019.00734

35. Smale DA. Impacts of ocean warming on kelp forest ecosystems. New Phytol. 2020; 225: 1447–1454. https://doi.org/10.1111/nph.16107 PMID: 31400287

36. Hoegh-Guldberg O. Climate change, coral bleaching and the future of the world's coral reefs. Mar Freshw Res. 1999; 50: 830–866. https://doi.org/10.1071/MF99078

37. Nepper-Davidsen J, Andersen D, Pedersen M. Effects of simulated heat wave scenarios on sugar kelp *Saccharina latissima*: exposure to high but sub-lethal temperatures causes long-term and partly irreversible reductions in performance. Mar Ecol Prog Ser. 2019; 630: 25–39.

38. Liesner D, Fouqueau L, Valero M, Roleda MY, Pearson GA, Bischof K, et al. Heat stress responses and population genetics of the kelp *Laminaria digitata* (Phaeophyceae) across latitudes reveal differentiation among North Atlantic populations. Ecol Evol. 2020; 10: 9144–9177. https://doi.org/10.1002/ece3.6569 PMID: 32953052

39. Umanzor S, Sandoval-Gil J, Sánchez-Barredo M, Ladah LB, Ramírez-García M, Zertuche-González JA. Short-term stress responses and recovery of giant kelp (*Macrocystis pyrifera*, Laminariales, Phaeophyceae) juvenile sporophytes to a simulated marine heatwave and nitrate scarcity. J Phycol. 2021; 57: 1604–1618. https://doi.org/10.1111/jpy.13189 PMID: 34124800

40. Graiff A, Liesner D, Karsten U, Bartsch I. Temperature tolerance of western Baltic Sea Fucus vesiculosus—growth, photosynthesis and survival. J Exp Mar Bio Ecol. 2015; 471: 8–16. https://doi.org/10.1016/j.jembe.2015.05.009

41. Gaitán-Espitia JD, Hancock JR, Padilla-Gamiño JL, Rivest EB, Blanchette CA, Reed DC, et al. Interactive effects of elevated temperature and *p*CO2 on early-life-history stages of the giant kelp *Macrocystis pyrifera*. J Exp Mar Bio Ecol. 2014; 457: 51–58. https://doi.org/10.1016/j.jembe.2014.03.018

42. Anthony KRN, Kline DI, Diaz-Pulido G, Dove S, Hoegh-Guldberg O. Ocean acidification causes bleaching and productivity loss in coral reef builders. Proc Natl Acad Sci. 2008; 105: 17442–17446. https://doi.org/10.1073/pnas.0804478105 PMID: 18988740

43. Martin S, Gattuso JP. Response of Mediterranean coralline algae to ocean acidification and elevated temperature. Glob Chang Biol. 2009; 15: 2089–2100. https://doi.org/10.1111/j.1365-2486.2009.01874.x

44. Cornwall CE, Comeau S, McCulloch MT. Coralline algae elevate pH at the site of calcification under ocean acidification. Glob Chang Biol. 2017; 23: 4245–4256. https://doi.org/10.1111/gcb.13673 PMID: 28370806

45. Martone PT, Alyono M, Stites S. Bleaching of an intertidal coralline alga: Untangling the effects of light, temperature, and desiccation. Mar Ecol Prog Ser. 2010; 416: 57–67. https://doi.org/10.3354/meps08782

46. Smale DA, Wernberg T. Ecological observations associated with an anomalous warming event at the Houtman Abrolhos Islands, Western Australia. Coral Reefs. 2012; 31: 441–441. https://doi.org/10.1007/s00338-012-0873-4

47. Pandolfi JM, Connolly SR, Marshall DJ, Cohen AL. Projecting coral reef futures under global warming and ocean acidification. Science. 2011; 333: 418–422. https://doi.org/10.1126/science.1204794 PMID: 21778392

48. Baker AC, Glynn PW, Riegl B. Climate change and coral reef bleaching: An ecological assessment of long-term impacts, recovery trends and future outlook. Estuar Coast Shelf Sci. 2008; 80: 435–471. https://doi.org/10.1016/j.ecss.2008.09.003

49. Hughes TP, Kerry JT, Baird AH, Connolly SR, Dietzel A, Eakin CM, et al. Global warming transforms coral reef assemblages. Nature. 2018; 556: 492–496. https://doi.org/10.1038/s41586-018-0041-2 PMID: 29670282

50. Hughes TP, Kerry JT, Álvarez-Noriega M, Álvarez-Romero JG, Anderson KD, Baird AH, et al. Global warming and recurrent mass bleaching of corals. Nature. 2017; 543: 373–377. https://doi.org/10.1038/nature21707 PMID: 28300113

51. Hughes TP, Anderson KD, Connolly SR, Heron SF, Kerry JT, Lough JM, et al. Spatial and temporal patterns of mass bleaching of corals in the Anthropocene. Science. 2018; 359: 80–83. https://doi.org/10.1126/science.aan8048 PMID: 29302011

52. Krieger Erik C., Nelson Wendy A., Grand Johan et al. The role of irradiance in controlling coralline algal calcification, 21 March 2022, PREPRINT (Version 1) available at Research Square [https://doi.org/10.21203/rs.3.rs-923640/v1]

53. Twist BA, Neill KF, Bilewitch J, Jeong SY, Sutherland JE, Nelson WA. High diversity of coralline algae in New Zealand revealed: Knowledge gaps and implications for future research. PLoS One. 2019; 14: 1–21. https://doi.org/10.1371/journal.pone.0225645 PMID: 31790447

54. Twist BA, Cornwall CE, McCoy SJ, Gabrielson PW, Martone PT, Nelson WA. The need to employ reliable and reproducible species identifications in coralline algal research. Mar Ecol Prog Ser. 2020; 654: 225–231. https://doi.org/10.3354/meps13506

55. Gattuso J-P, Magnan A, Billé R, Cheung WWL, Howes EL, Joos F, et al. Contrasting futures for ocean and society from different anthropogenic CO_2 emissions scenarios. Science. 2015;349. https://doi.org/10.1126/science.aac4722 PMID: 26138982

56. Dickson A. G., Sabine C. L. and Christian J. R. (Eds.) 2007. Guide to best practices for ocean CO2 measurements. PICES Special Publication 3, pp 191.

57. R Core Team. R: A language and environment for statistical computing. Vienna, Austria: R Foundation for Statistical Computing; 2021. Available: https://www.r-project.org/

58. Burdett HL, Hennige SJ, Francis FTY, Kamenos NA. The photosynthetic characteristics of red coralline algae, determined using pulse amplitude modulation (PAM) fluorometry. Bot Mar. 2012; 55: 499–509. https://doi.org/10.1515/bot-2012-0135

59. Williamson CJ, Brodie J, Goss B, Yallop M, Lee S, Perkins R. *Corallina* and *Ellisolandia* (Corallinales, Rhodophyta) photophysiology over daylight tidal emersion: interactions with irradiance, temperature and carbonate chemistry. Mar Biol. 2014; 161: 2051–2068. https://doi.org/10.1007/s00227-014-2485-8 PMID: 25170177

60. Sampath-Wiley P, Neefus CD. An improved method for estimating R-phycoerythrin and R-phycocyanin contents from crude aqueous extracts of *Porphyra* (Bangiales, Rhodophyta). J Appl Phycol. 2007; 19: 123–129. https://doi.org/10.1007/s10811-006-9118-7 PMID: 19396349

61. Ritchie RJ. Universal chlorophyll equations for estimating chlorophylls *a*, *b*, *c*, and *d* and total chlorophylls in natural assemblages of photosynthetic organisms using acetone, methanol, or ethanol solvents. Photosynthetica. 2008; 46: 115–126. https://doi.org/10.1007/s11099-008-0019-7

62. Jokiel P, Maragos J, Franzisket L. Coral growth: buoyant weight technique. Coral reefs Res methods. 1978; 529–541.

63. Comeau S, Cornwall CE, DeCarlo TM, Krieger E, McCulloch MT. Similar controls on calcification under ocean acidification across unrelated coral reef taxa. Glob Chang Biol. 2018; 24: 4857–4868. https://doi.org/10.1111/gcb.14379 PMID: 29957854

64. DeCarlo TM, Comeau S, Cornwall CE, Gajdzik L, Guagliardo P, Sadekov A, et al. Investigating marine bio-calcification mechanisms in a changing ocean with in vivo and high-resolution ex vivo Raman spectroscopy. Glob Chang Biol. 2019; 25: 1877–1888. https://doi.org/10.1111/gcb.14579 PMID: 30689259

65. DeCarlo TM D'Olivo JP, Foster T, Holcomb M, Becker T, McCulloch. Coral calcifying fluid aragonite saturation states derived from Raman spectroscopy. Biogeosciences. 2017; 14: 5253–5269. https://doi.org/10.5194/bg-14-5253-2017

66. Urmos J, Sharma SK, Mackenzie FT. Characterization of some biogenic carbonates with Raman spectroscopy. Am Mineral. 1991; 76: 641–646.

67. Perrin J, Vielzeuf D, Laporte D, Ricolleau A, Rossman GR, Floquet N. Raman characterization of synthetic magnesian calcites. Am Mineral. 2016; 101: 2525–2538. https://doi.org/10.2138/am-2016-5714

68. Marsh JA. Primary productivity of reef-building calcareous red algae. Ecology. 1970; 51. 2: 255–265.

69. Krieger Erik C., Taise Aleluia, Nelson Wendy A., Grand Johan, Eric Le Ru Simon K. Davy et al. Tolerance of coralline algae to ocean warming and marine heatwaves. 2022. Dryad Digital Repository. https://doi.org/10.5061/dryad.jwstqjqdh

70. Rendina F, Bouchet PJ, Appolloni L, Russo GF, Sandulli R, Kolzenburg R, et al. Physiological response of the coralline alga *Corallina officinalis* L. to both predicted long-term increases in temperature and short-term heatwave events. Mar Environ Res. 2019; 150: 104764. https://doi.org/10.1016/j.marenvres.2019.104764 PMID: 31376632

71. Ragazzola F, Marchini A, Adani M, Bordone A, Castelli A, Cerrati G, et al. An intertidal life: Combined effects of acidification and winter heatwaves on a coralline alga (*Ellisolandia elongata*) and its associated invertebrate community. Mar Environ Res. 2021; 169: 105342. https://doi.org/10.1016/j.marenvres.2021.105342 PMID: 33933902

72. Schubert N, Santos R, Silva J. Living in a Fluctuating Environment Increases Tolerance to Marine Heatwaves in the Free-Living Coralline Alga *Phymatolithon lusitanicum*. 2021; 8: 1–13. https://doi.org/10.3389/fmars.2021.791422

73. Biswal B, Joshi PN, Raval MK, Biswal UC. Photosynthesis, a global sensor of environmental stress in green plants: Stress signalling and adaptation. Curr Sci. 2011; 101: 47–56.

74. Mathur S, Agrawal D, Jajoo A. Photosynthesis: Response to high temperature stress. J Photochem Photobiol B Biol. 2014; 137: 116–126. https://doi.org/10.1016/j.jphotobiol.2014.01.010 PMID: 24796250

75. Jones RJ, Hoegh-Guldberg O, Larkum AWD, Schreiber U. Temperature-induced bleaching of corals begins with impairment of the CO_2 fixation mechanism in zooxanthellae. Plant, Cell Environ. 1998; 21: 1219–1230. https://doi.org/10.1046/j.1365-3040.1998.00345.x

76. Slavov C, Schrameyer V, Reus M, Ralph PJ, Hill R, Büchel C, et al. "Super-quenching" state protects *Symbiodinium* from thermal stress—Implications for coral bleaching. Biochim Biophys Acta—Bioenerg. 2016; 1857: 840–847. https://doi.org/10.1016/j.bbabio.2016.02.002 PMID: 26869375

77. Tchernov D, Gorbunov MY, De Vargas C, Yadav SN, Milligant AJ, Häggblom M, et al. Membrane lipids of symbiotic algae are diagnostic of sensitivity to thermal bleaching in corals. Proc Natl Acad Sci U S A. 2004; 101: 13531–13535. https://doi.org/10.1073/pnas.0402907101 PMID: 15340154

78. Zou M, Yuan L, Zhu S, Liu S, Ge J, Wang C. Effects of heat stress on photosynthetic characteristics and chloroplast ultrastructure of a heat-sensitive and heat-tolerant cultivar of wucai (*Brassica campestris* L.). Acta Physiol Plant. 2017; 39. https://doi.org/10.1007/s11738-016-2319-z

79. Salvucci ME, Crafts-Brandner SJ. Relationship between the heat tolerance of photosynthesis and the thermal stability of rubisco activase in plants from contrasting thermal environments. Plant Physiol. 2004; 134: 1460–1470. https://doi.org/10.1104/pp.103.038323 PMID: 15084731

80. Maynard JA, Turner PJ, Anthony KRN, Baird AH, Berkelmans R, Eakin CM, et al. ReefTemp: An interactive monitoring system for coral bleaching using high-resolution SST and improved stress predictors. Geophys Res Lett. 2008; 35: L05603. https://doi.org/10.1029/2007GL032175

81. Fisher PL, Malme MK, Dove S. The effect of temperature stress on coral–*Symbiodinium* associations containing distinct symbiont types. Coral Reefs. 2012; 31: 473–485. https://doi.org/10.1007/s00338-011-0853-0

82. McCulloch M, Falter J, Trotter J, Montagna P. Coral resilience to ocean acidification and global warming through pH up-regulation. Nat Clim Chang. 2012; 2: 623–627. https://doi.org/10.1038/nclimate1473

83. Burton EA, Walter LM. Relative precipitation rates of aragonite and Mg calcite from seawater: temperature or carbonate ion control? Geology. 1987; 15: 111–114. https://doi.org/10.1130/0091-7613(1987)15<111:RPROAA>2.0.CO;2

84. Kamenos NA, Law A. Temperature controls on coralline algal skeletal growth. J Phycol. 2010; 46: 331–335. https://doi.org/10.1111/j.1529-8817.2009.00780.x

85. Pörtner HO. Integrating climate-related stressor effects on marine organisms: Unifying principles linking molecule to ecosystem-level changes. Mar Ecol Prog Ser. 2012; 470: 273–290. https://doi.org/10.3354/meps10123

86. Anton A, Randle JL, Garcia FC, Rossbach S, Ellis JI, Weinzierl M, et al. Differential thermal tolerance between algae and corals may trigger the proliferation of algae in coral reefs. Glob Chang Biol. 2020; 26: 4316–4327. https://doi.org/10.1111/gcb.15141 PMID: 32364636

87. Comeau S, Cornwall CE, Pupier CA, DeCarlo TM, Alessi C, Trehern R, et al. Flow-driven micro-scale pH variability affects the physiology of corals and coralline algae under ocean acidification. Sci Rep. 2019; 9: 1–12. https://doi.org/10.1038/s41598-019-49044-w PMID: 31492930

88. Kamenos NA, Cusack M, Moore PG. Coralline algae are global palaeothermometers with bi-weekly resolution. Geochim Cosmochim Acta. 2008; 72: 771–779. https://doi.org/10.1016/j.gca.2007.11.019

89. Halfar J, Zack T, Kronz A, Zachos JC. Growth and high-resolution paleoenvironmental signals of rhodoliths (coralline red algae): A new biogenic archive. J Geophys Res Ocean. 2000; 105: 22107–22116. https://doi.org/10.1029/1999JC000128

90. Henrich R, Freiwald A, Wehrmann A, Schäfer P, Samtleben C, Zankl H. Nordic cold-water carbonates: occurrences and controls. Glob Reg Control Biog Sediment Göttinger Arb zur Geol und Paläontologie, Sonderband. 1996; 2: 35–52.

91. Williams S, Adey W, Halfar J, Kronz A, Gagnon P, Bélanger D, et al. Effects of light and temperature on Mg uptake, growth, and calcification in the proxy climate archive *Clathromorphum compactum*. Biogeosciences. 2018; 15: 5745–5759. https://doi.org/10.5194/bg-15-5745-2018

92. Moberly R. Composition of magnesian calcites of algae and pelecypods by electron microprobe analysis. Sedimentology. 1968; 11: 61–82. https://doi.org/10.1111/j.1365-3091.1968.tb00841.x

93. Nash MC, Diaz-Pulido G, Harvey AS, Adey W. Coralline algal calcification: A morphological and process-based understanding. PLoS One. 2019; 14: e0221396. https://doi.org/10.1371/journal.pone.0221396 PMID: 31557180

94. Perry CT, Alvarez-Filip L. Changing geo-ecological functions of coral reefs in the Anthropocene. Graham N, editor. Funct Ecol. 2018; 33.6: 976–988. https://doi.org/10.1111/1365-2435.13247

95. Hind KR, Starko S, Burt JM, Lemay MA, Salomon AK, Martone PT. Trophic control of cryptic coralline algal diversity. Proc Natl Acad Sci. 2019; 116: 15080–15085. https://doi.org/10.1073/pnas.1900506116 PMID: 31285351

96. Wahid A, Gelani S, Ashraf M, Foolad MR. Heat tolerance in plants: An overview. Environ Exp Bot. 2007; 61: 199–223. https://doi.org/10.1016/j.envexpbot.2007.05.011

97. Murata N, Takahashi S, Nishiyama Y, Allakhverdiev SI. Photoinhibition of photosystem II under environmental stress. Biochim Biophys Acta—Bioenerg. 2007; 1767: 414–421. https://doi.org/10.1016/j.bbabio.2006.11.019 PMID: 17207454

98. Sharkey TD. Effects of moderate heat stress on photosynthesis: Importance of thylakoid reactions, rubisco deactivation, reactive oxygen species, and thermotolerance provided by isoprene. Plant, Cell Environ. 2005; 28: 269–277. https://doi.org/10.1111/j.1365-3040.2005.01324.x

99. Salvucci ME, Crafts-Brandner SJ. Inhibition of photosynthesis by heat stress: The activation state of Rubisco as a limiting factor in photosynthesis. Physiol Plant. 2004; 120: 179–186. https://doi.org/10.1111/j.0031-9317.2004.0173.x PMID: 15032851

100. Tabita FR, Satagopan S, Hanson TE, Kreel NE, Scott SS. Distinct form I, II, III, and IV Rubisco proteins from the three kingdoms of life provide clues about Rubisco evolution and structure/function relationships. J Exp Bot. 2008; 59: 1515–1524. https://doi.org/10.1093/jxb/erm361 PMID: 18281717

101. Iñiguez C, Galmés J, Gordillo FJL. Rubisco carboxylation kinetics and inorganic carbon utilization in polar versus cold-temperate seaweeds. J Exp Bot. 2019; 70: 1283–1297. https://doi.org/10.1093/jxb/ery443 PMID: 30576461

102. Tcherkez GGB, Farquhar GD, Andrews TJ. Despite slow catalysis and confused substrate specificity, all ribulose bisphosphate carboxylases may be nearly perfectly optimized. Proc Natl Acad Sci. 2006; 103: 7246–7251. https://doi.org/10.1073/pnas.0600605103 PMID: 16641091

103. Uemura K, Anwaruzzaman, Miyachi S, Yokota A. Ribulose-1,5-bisphosphate carboxylase/oxygenase from thermophilic red algae with a strong specificity for CO_2 fixation. Biochem Biophys Res Commun. 1997; 233: 568–571. https://doi.org/10.1006/bbrc.1997.6497 PMID: 9144578

104. Whitney SM, Andrews TJ. The CO_2/O_2 specificity of single-subunit ribulose-bisphosphate carboxylase from the dinoflagellate, *Amphidinium carterae*. Aust J Plant Physiol. 1998; 25: 131–138. https://doi.org/10.1071/PP97131

105. Hagemann M, Bauwe H. Photorespiration and the potential to improve photosynthesis. Curr Opin Chem Biol. 2016; 35: 109–116. https://doi.org/10.1016/j.cbpa.2016.09.014 PMID: 27693890

106. Galmés J, Conesa MÀ, Díaz-Espejo A, Mir A, Perdomo JA, Niinemets Ü, et al. Rubisco catalytic properties optimized for present and future climatic conditions. Plant Sci. 2014; 226: 61–70. https://doi.org/10.1016/j.plantsci.2014.01.008 PMID: 25113451

107. Gantt E. Phycobilisomes Ann Rev Plant Physiol. 1981; 327–347.

108. Patty CHL, Ariese F, Buma WJ, ten Kate IL, van Spanning RJM, Snik F. Circular spectropolarimetric sensing of higher plant and algal chloroplast structural variations. Photosynth Res. 2019; 140: 129–139. https://doi.org/10.1007/s11120-018-0572-2 PMID: 30141032

109. Anderson JM. Insights into the consequences of grana stacking of thylakoid membranes in vascular plants: a personal perspective. Funct Plant Biol. 1999; 26: 625. https://doi.org/10.1071/PP99070

110. Anderson JM, Chow WS, De Las Rivas J. Dynamic flexibility in the structure and function of photosystem II in higher plant thylakoid membranes: the grana enigma. Photosynth Res. 2008; 98: 575–587. https://doi.org/10.1007/s11120-008-9381-3 PMID: 18998237

111. Chow WS, Kim EH, Horton P, Anderson JM. Granal stacking of thylakoid membranes in higher plant chloroplasts: The physicochemical forces at work and the functional consequences that ensue. Photochem Photobiol Sci. 2005; 4: 1081–1090. https://doi.org/10.1039/b507310n PMID: 16307126

112. Kirchhoff H, Sharpe RM, Herbstova M, Yarbrough R, Edwards GE. Differential mobility of pigment-protein complexes in granal and agranal thylakoid membranes of C3 and C4 plants. Plant Physiol. 2013; 161: 497–507. https://doi.org/10.1104/pp.112.207548 PMID: 23148078

113. Kirchhoff H. Dynamic Architecture of Plant Photosynthetic Membranes. Plastid Biology. New York, NY: Springer New York; 2014. pp. 129–154. https://doi.org/10.1007/978-1-4939-1136-3_5

114. Nagy G, Ünnep R, Zsiros O, Tokutsu R, Takizawa K, Porcar L, et al. Chloroplast remodeling during state transitions in *Chlamydomonas reinhardtii* as revealed by noninvasive techniques in vivo. 2014;111. https://doi.org/10.1073/pnas.1322494111 PMID: 24639515

115. Chuartzman SG, Nevo R, Shimoni E, Charuvi D, Kiss V, Ohad I, et al. Thylakoid Membrane Remodeling during State Transitions in *Arabidopsis*. Plant Cell. 2008; 20: 1029–1039. https://doi.org/10.1105/tpc.107.055830 PMID: 18398051

116. Zhang R, Wise RR, Struck KR, Sharkey TD. Moderate heat stress of *Arabidopsis thaliana* leaves causes chloroplast swelling and plastoglobule formation. Photosynth Res. 2010; 105: 123–134. https://doi.org/10.1007/s11120-010-9572-6 PMID: 20563644

117. Ristic Z, Cass DD. Chloroplast Structure after Water Shortage and High Temperature in Two Lines of *Zea mays* L. that Differ in Drought Resistance. Bot Gaz. 1991; 152: 186–194. https://doi.org/10.1086/337878

118. Zhang RD, Zhou YF, Yue ZX, Chen XF, Cao X, Xu XX, et al. Changes in photosynthesis, chloroplast ultrastructure, and antioxidant metabolism in leaves of sorghum under waterlogging stress. Photosynthetica. 2019; 57: 1076–1083. https://doi.org/10.32615/ps.2019.124

119. Fristedt R, Willig A, Granath P, Crèvecoeur M, Rochaix J-D, Vener A V. Phosphorylation of Photosystem II Controls Functional Macroscopic Folding of Photosynthetic Membranes in *Arabidopsis*. Plant Cell. 2010; 21: 3950–3964. https://doi.org/10.1105/tpc.109.069435 PMID: 20028840

120. Derks A, Schaven K, Bruce D. Diverse mechanisms for photoprotection in photosynthesis. Dynamic regulation of photosystem II excitation in response to rapid environmental change. Biochim Biophys Acta—Bioenerg. 2015; 1847: 468–485. https://doi.org/10.1016/j.bbabio.2015.02.008 PMID: 25687894

121. Kirilovsky D, Kaňa R, Prášil O. Mechanisms Modulating Energy Arriving at Reaction Centers in Cyanobacteria. In: Demmig-Adams B, Garab G, Adams W III, Govindjee, editors. Dordrecht: Springer Netherlands; 2014. pp. 471–501. https://doi.org/10.1007/978-94-017-9032-1_22